ANNUAL REVIEWS

Annual Review of Nuclear and Particle Science

What Is the Top Quark Mass?

André H. Hoang[1,2]

[1]Faculty of Physics, University of Vienna, A-1090 Vienna, Austria;
email: andre.hoang@univie.ac.at

[2]Erwin Schrödinger International Institute for Mathematical Physics, A-1090 Vienna, Austria

Annu. Rev. Nucl. Part. Sci. 2020. 70:225–55

First published as a Review in Advance on July 24, 2020

The *Annual Review of Nuclear and Particle Science* is online at nucl.annualreviews.org

https://doi.org/10.1146/annurev-nucl-101918-023530

Keywords

top quark mass measurements, renormalization schemes, Monte Carlo event generators

Abstract

This review provides an overview of the conceptual issues regarding the interpretation of so-called direct top quark mass measurements, which are based on the kinematic reconstruction of top quark decay products at the Large Hadron Collider (LHC). These measurements quote the top mass parameter $m_t^{\rm MC}$ of Monte Carlo event generators with current uncertainties of around 0.5 GeV. The problem of finding a rigorous relation between $m_t^{\rm MC}$ and top mass renormalization schemes defined in field theory is unresolved to date and touches perturbative as well as nonperturbative aspects and the limitations of state-of-the-art Monte Carlo event generators. I review the status of LHC top mass measurements, illustrate how conceptual limitations enter the picture, and explain a controversy that has permeated the community in the context of the interpretation problem related to $m_t^{\rm MC}$. I then summarize recent advances in acquiring first principles insights and outline what else has to be understood to fully resolve the issue. I conclude with recommendations on how to deal with the interpretation problem for the time being when making top mass–dependent theoretical predictions.

Contents

1. INTRODUCTION

The top quark is the heaviest particle in the Standard Model of elementary particle physics (SM). The currently most precise determinations of its mass come from so-called direct measurements. These measurements are based on the experimental kinematic reconstruction of the final-state top quark decay products (i.e., bottom quark jets, light quark jets from W boson decays, and leptons) and the comparison of kinematic distributions one can construct from the four-momenta of the decay products with descriptions of the same quantities obtained from multipurpose Monte Carlo event generators (MMCs). They determine the top mass parameter of the MMC and yield a world average of $m_t^{\rm MC} = 172.9 \pm 0.4$ GeV (1) with an impressive relative precision of 0.2%, making the top quark mass the most precisely known parameter in the strong interaction sector of the SM, quantum chromodynamics (QCD). For the high-luminosity phase of the Large Hadron Collider (HL-LHC), it is projected that uncertainties as small as 200 MeV can be reached from direct top mass measurements (2).

The major portion of the top quark's mass is generated through the electroweak Higgs mechanism (3–5), which also gives all other elementary particles of the SM their masses. The precise knowledge of the elementary particle masses and their couplings is an important element in consistency tests of the SM and in indirect searches of physics beyond the SM. Because the hopes for discoveries of non-SM elementary particles at the LHC have not been fulfilled to date, indirect New Physics searches, which focus on finding deviations between experimental data and SM predictions, have become increasingly important. These searches require a high level of precision and a thorough and systematic understanding of subtle experimental as well as theoretical issues. In this context, the top quark plays a special role because its large mass makes it a highly sensitive probe of the structure of the SM Higgs sector and an important ingredient in models of physics beyond the SM. In this context, it is the electroweak part of the top quark mass one seeks to know with the highest possible precision. It is frequently stated that because of its small lifetime $[1/\tau_t = \Gamma_t = 1.42^{+0.19}_{-0.15}$ GeV (1)], the top quark, despite its strong color charge, is protected from low-scale hadronization effects and behaves more or less as a free particle.

The results for $m_t^{\rm MC}$ obtained from the direct measurements have often been identified with the so-called top quark pole mass $m_t^{\rm pole}$, which is a popular renormalization scheme used for

SM: Standard Model of elementary particle physics

MMC: multipurpose Monte Carlo event generator

QCD: quantum chromodynamics

HL-LHC: high-luminosity phase of the Large Hadron Collider

LHC: Large Hadron Collider

perturbative QCD computations at next-to-leading order (NLO) and beyond. The pole mass encodes, strictly within perturbation theory, the notion of the kinematic rest mass of the top quark as a real on-shell particle. The identification seems natural because the top mass sensitivity of the kinematic distributions entering the direct measurement analyses is coming from resonance and endpoint structures that can be seen as related to the kinematic properties of a top quark particle with a definite mass. I refer to distributions of this kind as observables with kinematic (top) mass sensitivity. With the identification of m_t^{MC} and m_t^{pole}, precise higher-order predictions for the SM electroweak potential (6–10) have been made. These predictions, together with precise measurements of the Higgs boson mass (1), indicate that the SM is in a metastable state.[1] However, in recent years a discussion has emerged as to whether, considering a precision of 0.5 GeV or better, the available NLO (and higher-order) perturbative calculations and NLO-matched MMCs indeed control the QCD dynamics that affects the top quark mass, and the way in which direct measurement observables depend on it, sufficiently to justify the identification of m_t^{MC} with the pole mass (7, 12–23). In this context, the direct measurements, being the most precise and known to rely essentially entirely on the parton shower (PS) and hadronization dynamics of the MMCs, have received the most attention. I call the associated set of physical issues the top mass "interpretation problem." The top mass interpretation problem is a question of the precise relation between m_t^{MC} and more fundamental and field-theoretic mass definitions, such as the pole mass, the $\overline{\mathrm{MS}}$ mass, and other mass schemes. The origin of the problem is that the simple picture of a free top quark, which directly governs the visible structures in distributions with kinematic top mass sensitivity, is too naive, and the effects of QCD and electroweak quantum fluctuations must be accounted for with high precision. These quantum effects are governed by low-energy scales at the level of 1 GeV even though the top mass is extremely large, and they can directly affect the extracted top mass if they are not described theoretically in an adequate way. What makes matters subtle is that the low-energy QCD dynamics is difficult to control theoretically because of large higher-order perturbative corrections and nonperturbative effects. The top mass interpretation problem emerges because the top mass–sensitive kinematic distributions used for the direct measurements are so complicated that, with the current technology, their theoretical description can only be provided by MMCs. In the current generation of MMCs, however, the theoretical precision and quality of the low-energy PS and hadronization dynamics cannot yet be systematically controlled at a level such that the identification of the top mass parameter m_t^{MC} with a field-theoretic mass scheme such as the pole mass can be proven from first principles.

Probably the most confusing aspect of the emerging discussions has been the lack of consensus on how to estimate and even formulate the uncertainty associated with the top mass interpretation problem and how to deal with it in practical applications (see, e.g., Reference 2). Furthermore, the issue has not been discussed in a coherent fashion in the community, and the advocated points of view have shifted slightly over time. I call this aspect of the interpretation problem "the controversy" because it is related to different views of the relevance of the physical aspects of the interpretation problem but does not contribute in any way to a resolution of the physical questions. Meanwhile, a number of alternative top mass measurement methods have been devised for the LHC, motivated in part by the idea of applying methods that are unaffected or affected in a different way by the interpretation problem. These methods are still less precise than the direct measurements and have their own subtleties once their precision increases. The situation is

NLO: next-to-leading-order approximation in fixed-order perturbation theory

PS: parton shower

$\overline{\mathrm{MS}}$: conventional minimal subtraction scheme within dimensional regularization

[1]The coupling of the top quark to the Higgs boson generates the large electroweak portion of the mass of the top quark. The top quark mass conversely causes large quantum corrections to the Higgs self-coupling, which determines the Higgs boson mass and also the stability properties of the potential for the Higgs boson field and the SM vacuum. These quantum effects decrease the Higgs self-coupling for a larger top mass with the possibility of destabilizing the vacuum (11).

reflected in an interesting way in the *Review of Particle Physics* (1), in which the top quark is the only quark for which three different masses are quoted in the particle listings. However, it should be clearly emphasized that in hadron–hadron collisions, in which the hard interactions that underlie the observables unavoidably involve partons in nonsinglet color configurations, the conceptual issues that affect the direct measurements will eventually emerge for all top mass measurements methods once a precision of 0.5 GeV or better is reached.

NLL: next-to-leading-order approximation in logarithm-resummed perturbation theory

The interpretation problem consists of a complex set of issues and requires significant theoretical progress on multiple fronts, predominantly beyond the realm of fixed-order perturbative calculations. The issue can be resolved in a straightforward and fully transparent way only after, at the least, next-to-leading logarithmic (NLL) precise PSs and MMCs have become available (for the observables entering the top mass measurements). These new-generation MMCs should be capable of describing the top quark decay and the nonperturbative aspects of color neutralization in a systematic manner such that the field theory aspects of the MMC top mass parameter (and even the strong coupling parameter) are well defined and can be determined from a simple computation. Such developments clearly require a dedicated and long-term effort that will also benefit all other aspects of collider physics. Even if such an outlook is overly optimistic, much can be learned from addressing these issues through dedicated studies to help resolve the controversy at least partially for some of the direct top mass measurement methods.

In this review, I explain the questions involved in the top mass interpretation problem from a physical and conceptual perspective. I hope the review enables a better understanding of the physical and systematic aspects of the interpretation problem (and also the controversy) and an appreciation of the problems to be resolved. I attempt to be as nontechnical as possible, but the problem is of a subtle theoretical nature. For simplicity, all formulas shown are either understood as qualitative or truncated at $\mathcal{O}(\alpha_s)$ or NLO, even though higher-order corrections are known in most cases. All numerical results quoted have been computed, including all available higher-order corrections; I use $\alpha_s^{(n_\ell=5)}(M_Z) = 0.118$ as the reference input for the strong coupling. I apologize for any references that have been omitted, either unintentionally or for reasons of space.

The review is organized as follows. In Section 2, the physical aspects of different top quark renormalization schemes are reviewed. This section serves as a basis for the following discussions. However, I emphasize that a mere discussion of top mass schemes does not resolve the top mass interpretation problem. Section 3 provides an overview of the current status of top quark mass measurements and the theoretical tools employed. In this section, I focus on the limitations of the theoretical tools, which are the origin of the top mass interpretation problem, and the role these theoretical tools play in the other top mass measurement methods. In Section 4, I phrase the controversy in a set of formulas that can be discussed in a concrete way. Section 5 reviews recent work that quantifies the interpretation problem numerically. In particular, I discuss the recent work described in Reference 24, in which some first conceptual and concrete analytical insights into the perturbative (parton-level) aspects of the interpretation problem were gained. Finally, in Section 6, I summarize and conclude with a practical recommendation on how to deal with the top mass interpretation problem at this time.

2. MASS EXTRACTION AND RENORMALIZATION SCHEMES

2.1. The Principle of Top Mass Determinations

Since the top quark—like all other quarks that carry strong interaction color charge—is not a physically observable particle, its mass is a quantity that needs to be defined from a theoretical prescription in quantum field theory, which is called a renormalization scheme or a mass scheme.

The choice of scheme is in principle arbitrary. The usefulness and systematics of this concept arise from our ability to make precise predictions for a physical observable in a given scheme and to relate the predictions in different schemes to each other by theoretical calculations. Because contemporary high-energy physics for the most part considers observables for which perturbative computations can be used, usually only quark mass schemes that are defined strictly within perturbation theory are considered. This view is commonly accepted in high-energy collider physics, and I also adopt it in this review. So, given two top mass schemes (called m_t^A and m_t^B), the relation between the two can be described by a perturbative series of the form

$$m_t^A - m_t^B = \sum_{n=1} c_n \alpha_s^n(\mu). \qquad 1.$$

For simplicity, I only indicate powers of the strong coupling α_s and suppress contributions from the electromagnetic and weak couplings. The precision of the relation is limited by the ability to calculate and then to evaluate the truncated series in a meaningful way. I emphasize this point because perturbative series in non-Abelian gauge theories such as QCD are in general asymptotic and not convergent. I return to this point in Section 2.2 in my discussion of the pole mass scheme. Given a top mass–sensitive observable σ, where I mostly refer to different kinds of cross sections, the corresponding perturbative (and also asymptotic) series, called the parton-level cross section, can be written as $\hat{\sigma}(Q, m_t^X, \alpha_s(\mu), \mu; \delta m^X)$. The energy Q of the process, the top mass m_t^X in scheme X, the strong coupling $\alpha_s(\mu)$, and the dependence on the renormalization scale μ appear as explicit arguments. Furthermore, the separated argument δm^X stands for the dependence of the series on the scheme choice X. By construction, the perturbative series in the two mass schemes are formally equivalent:[2]

$$\hat{\sigma}(Q, m_t^A, \alpha_s(\mu), \mu; \delta m^A) = \hat{\sigma}(Q, m_t^B, \alpha_s(\mu), \mu; \delta m^B). \qquad 2.$$

However, in practice they differ because of the truncation of the series and our limited ability to calculate and sum the series.

The freedom of scheme also exists for the strong coupling α_s. Within the commonly accepted paradigm of using dimensional regularization and the so-called $\overline{\text{MS}}$ prescription for α_s (which are explained in Section 2.2), this freedom is signified by the dependence on the renormalization scale μ. A useful aspect of the coupling $\alpha_s(\mu)$ is that one can interpret μ as the momentum scale above which all quantum corrections to the fundamental QCD gluon interactions are absorbed into $\alpha_s(\mu)$. So, for the choice $\mu \sim Q$ (in particular when $Q \gg m_t$), the resulting perturbation series often behave quite well. In this way, an important set of logarithmic corrections is also summed up to all orders in perturbation theory. The numerical differences between different considered reasonable scheme choices are then typically used to estimate the theoretical uncertainties of the parton-level cross section.

However, for the extraction of the top mass (and any other QCD parameter) from an experimentally measured cross section σ^{exp}, the parton-level cross section does not provide the full answer, and it is necessary to account for nonperturbative corrections:

$$\sigma^{\text{exp}} = \hat{\sigma}(Q, m_t^X, \alpha_s(\mu), \mu; \delta m^X) + \sigma^{\text{NP}}(Q, \Lambda_{\text{QCD}}). \qquad 3.$$

Here, Λ_{QCD} stands for a nonperturbative scale with typical size of a few hundred MeV that governs the magnitude of the nonperturbative correction σ^{NP}. The form of Equation 3 is schematic and also accounts for the nonperturbative effects in the parton distribution functions needed to calculate cross sections at the LHC. For most cross sections, one has $Q \gg \Lambda_{\text{QCD}}$ and typically

Λ_{QCD}: scheme-dependent nonperturbative hadronization scale, typically around 200 MeV

[2] I suppress the dependence on the masses of other quarks or leptons.

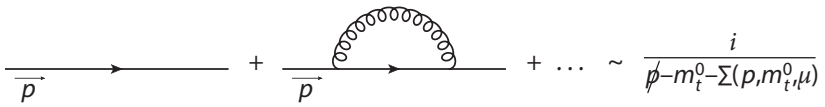

Figure 1

Self-energy at next-to-leading order for the top quark with four-momentum p^μ.

$\hat{\sigma} > \sigma^{\mathrm{NP}}$. Since we consider mass schemes that are strictly defined within perturbation theory, the relations between mass schemes shown in Equation 1 are free of nonperturbative corrections, such that switching between mass schemes does not modify the structure or the content of σ^{NP}. The precision for the top mass extraction depends on the ability to calculate the perturbative cross section $\hat{\sigma}$ and to determine the nonperturbative correction σ^{NP}. Likewise, the uncertainty in the extracted top mass arises from the combined uncertainties in $\hat{\sigma}$ and σ^{NP}; one must keep in mind that σ^{NP} itself is not responsible for the top mass dependence of the observable σ^{exp}. The most preferred observables for top mass measurements (and in general) are those in which σ^{NP} vanishes as $(\Lambda_{\mathrm{QCD}}/Q)^n$, with $n \geq 2$ for the limit $\Lambda_{\mathrm{QCD}}/Q \to 0$, because then the contributions of σ^{NP} can be very small (since $Q, m_t \gg \Lambda_{\mathrm{QCD}}$). An example of such a "clean" observable is the total inclusive $t\bar{t}$ cross section in e^+e^- annihilation, for which the observable-initiating hard reaction is the production of a color-singlet $t\bar{t}$ pair via the process $e^+e^- \to \gamma, Z \to t\bar{t}$.[3] Here, $n = 4$, and the nonperturbative corrections are negligible for most applications. Unfortunately, at the LHC, such clean cross sections do not exist because nonsinglet color configurations are unavoidable for the observable-initiating hard reactions when partons (i.e., quarks and gluons that emerge from the colliding protons) appear in the scattering initial state and when jet formation is crucial for the construction of an observable. Therefore, color neutralization processes that are linearly sensitive to soft and nonperturbative momenta are unavoidable, and σ^{NP} always depends linearly on Λ_{QCD}. Thus, σ^{NP} cannot be disregarded in experiments at the LHC.

2.2. Top Mass Renormalization Schemes

In analogy to adopting an adequate choice for the renormalization scale μ of the strong coupling $\alpha_s(\mu)$, one also adopts an adequate top quark mass scheme. The central formal aspect of top quark mass renormalization is to absorb the ultraviolet (UV) divergence that arises in the NLO self-energy diagram (see the generic illustration in **Figure 1**). Here,

$$\Sigma(p, m_t^0, \mu) \sim m_t^0 \left(\frac{\alpha_s(\mu)}{\pi}\right)\left[\frac{1}{\epsilon} + \ln(4\pi e^{-\gamma_E}) + A^{\mathrm{fin}}(m_t^0/\mu)\right] + \ldots \qquad 4.$$

displays the dominant contribution in the resonance limit $p^2 \to m_t^2$ within a calculation in $d = 4 - 2\epsilon$ space-time dimensions. Using d dimensions is the standard way to regularize UV divergences in perturbative QCD computations and is called dimensional regularization. The ellipsis indicates higher-order corrections proportional to higher powers of the strong coupling α_s, which are known to $\mathcal{O}(\alpha_s^4)$ (36–41). The term that is divergent in the limit $\epsilon \to 0$ (which quantifies the UV divergence to be renormalized) and the finite term $A^{\mathrm{fin}}(m_t^0/\mu)$ are shown separately, and m_t^0

UV: ultraviolet (referring to large momenta or energies)

[3]The inclusive $t\bar{t}$ cross section in e^+e^- annihilation at center-of-mass energies Q close to the production threshold, $Q \approx 2m_t$, constitutes the most precise top mass measurement method at a future e^+e^- collider. Theoretical cross-section predictions (25–30) have reached uncertainties at the level of several percent and allow for top mass determinations with uncertainties at the level of 50 MeV or better (31–34). Because the production of $t\bar{t}$ pairs in color-octet configurations is strongly suppressed, the effects of soft QCD radiation are strongly suppressed as well. This suppression also applies to the $t\bar{t}\gamma$ final state analyzed in Reference 35.

indicates the bare unrenormalized mass. In this context, the term $A^{\rm fin}$, despite being finite, contains a contribution from self-energy quantum fluctuations that arise from soft (i.e., small) momenta in a top resonance frame.[4] These soft quantum corrections, which I refer to in Section 5.2 as ultracollinear corrections, affect $m_t^0 A^{\rm fin}(m_t^0/\mu)$ linearly (42, 43). For example, giving the gluon a small test mass λ, which cuts off these soft momenta, one obtains (44)

$$m_t^0 A^{\rm fin}(m_t^0/\mu)\big|_{\rm gluonmass\,\lambda} = m_t^0 A^{\rm fin}(m_t^0/\mu)\big|_{\lambda=0} + \frac{2}{3}\lambda + \mathcal{O}(\lambda^2/m_t^0). \qquad 5.$$

This relation should be remembered in the following sections because perturbation theory does not work well in this regime.

The mass scheme that is closest to the concept of the strong coupling $\alpha_s(\mu)$ is the $\overline{\rm MS}$ scheme $\overline{m}_t(\mu)$. Here, only the pure UV $1/\epsilon$ term [including the conventional term $\ln(4\pi e^{-\gamma_E})$] is absorbed into the renormalized mass:

$$\overline{m}_t(\mu) = m_t^0 \left\{1 + \left(\frac{\alpha_s(\mu)}{\pi}\right)\left[\frac{1}{\epsilon} + \ln(4\pi e^{-\gamma_E})\right]\right\} + \ldots. \qquad 6.$$

The $\overline{\rm MS}$ mass is μ-dependent like $\alpha_s(\mu)$ and satisfies the renormalization group equation

$$\frac{\rm d}{{\rm d}\ln\mu}\,\overline{m}_t(\mu) = -\overline{m}_t(\mu)\left(\frac{\alpha_s(\mu)}{\pi}\right) + \ldots, \qquad 7.$$

implying that $\overline{m}_t(\mu)$ depends logarithmically on μ. In analogy to $\alpha_s(\mu)$, we can interpret μ as the momentum scale (in a top resonance frame) above which all self-energy quantum corrections are absorbed into $\overline{m}_t(\mu)$ (see **Figure 2** for a graphical illustration). The $\overline{\rm MS}$ mass is therefore not affected by low-energy or nonperturbative quantum fluctuations and is called a short-distance mass. The term $A^{\rm fin}$ in Equation 4, which is not absorbed into the renormalized mass, still appears in the perturbative calculations of the process, and its "bad" linearly sensitive small-momentum contributions are known to cancel with other virtual (nonself-energy) corrections that are soft in a top resonance frame. This cancellation can be explicitly checked for any parton-level cross section for a physical process involving top quarks by considering the sum of all linear gluon mass terms as that displayed for $A^{\rm fin}$ in Equation 5 coming from radiation that is soft in a top resonance frame. Setting μ to the physical scale of the process governing the mass dependence of an observable, together with a proper scale setting for the strong coupling, frequently yields good behavior for the perturbation series of $\hat{\sigma}$. However, the interpretation of $\overline{m}_t(\mu)$ just mentioned applies only for observables where $\mu \gtrsim m_t$ (which includes, e.g., total inclusive cross sections at very high energies $Q \gg m_t$) or when the top effects are virtual, such as for the SM Higgs potential (6–10), the electroweak precision observables (1, 45), and the properties of B mesons (46). Such observables can have a strong indirect top mass sensitivity but not a kinematic mass sensitivity.

As mentioned in Section 1, observables with kinematic mass sensitivity are related to distributions of variables that show sharp threshold patterns, such as resonances, shoulders, and endpoints. Even though these patterns are initiated by hard reactions that involve the large scales m_t or Q, the observable mass dependence is also modified by dynamical QCD and electroweak quantum effects. The momentum scales governing these quantum effects are, however, soft—that is, much smaller than m_t. I refer to these momentum scales generically as the scale R. So, for observables with kinematic mass sensitivity, we typically have $R \ll m_t$. The prototypical example is the invariant mass of jets coming from the hadronic decay of a top quark. Here, the scale R

[4]In this reference frame, a top quark state within its finite-lifetime Breit–Wigner resonance region has a nonrelativistic average velocity. Such frames often are collectively called the top quark rest frame, but I do not adopt this jargon in this review because it is not appropriate when discussing uncertainties in mass determinations much smaller than the top quark width $\Gamma_t(t \to bW) = 1.4$ GeV.

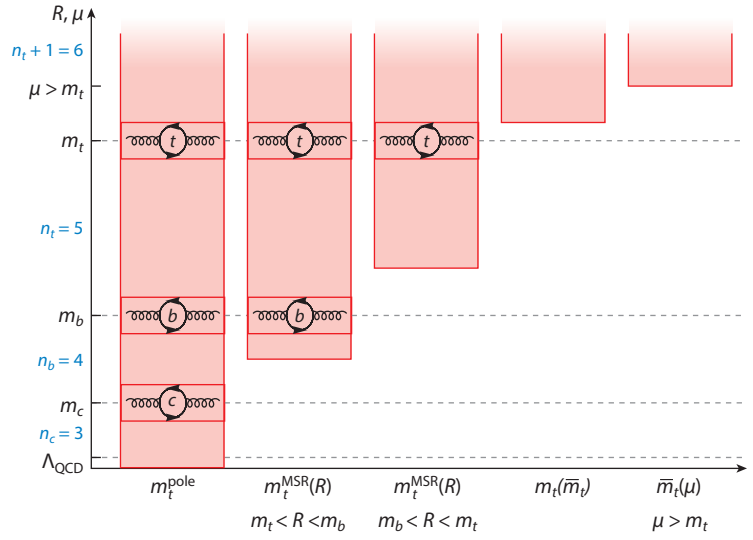

Figure 2

The red shaded regions represent the self-energy contributions absorbed into the pole mass $m_t^{\rm pole}$, MSR mass $m_t^{\rm MSR}(R)$, and $\overline{\rm MS}$ mass $\overline{m}_t(\mu)$. The pole mass absorbs all contributions down to vanishing momenta, whereas the MSR and $\overline{\rm MS}$ masses absorb only contributions above the scales R and μ, respectively. Figure adapted from Reference 47 (CC BY 4.0).

governing the soft quantum effects discussed above is set by the width of the resonance visible in the invariant mass distribution. It is bounded from below by the top width Γ_t or the experimental resolution. **Figure 3*a*** shows the top mass dependence of the reconstructed top invariant mass $m_t^{\rm reco}$ from LHC simulations carried out in Reference 48. The distribution in this case shows an R of around 30 GeV. The high mass sensitivity arises from the location of the resonance structure. While the basic location and existence of the resonance are tied to the top quark mass, which is large, the details of the resonance shape, its width, and the exact location are also governed by low-energy QCD and electroweak effects. Observables of this kind form the basis of the direct top mass measurements.

To define an adequate scale-dependent short-distance mass for observables where the mass sensitivity is affected by QCD dynamics with momentum scales $R < m_t$, one switches to an effective description in analogy to the well-known Foldy–Wouthuysen transformation (49). Here, the virtual off-shell and hard top quark quantum effects are also absorbed into the mass (or integrated out) but without absorbing the soft top quark dynamics. A mass scheme that realizes this concept is the MSR scheme $m^{\rm MSR}(R)$ (47, 50, 51), which is defined for $R < m_t$ by the relation

$$m_t^{\rm MSR}(R) = m_t^0 \left\{1 + \left(\frac{\alpha_s(R)}{\pi}\right)\left[\frac{1}{\epsilon} + \ln(4\pi e^{-\gamma_E}) + A^{\rm fin}(m_t^0/R)\right]\right\} - R\left(\frac{\alpha_s(R)}{\pi}\right)A^{\rm fin}(1) + \ldots. \quad 8.$$

MSR: renormalization scheme including power corrections down to the soft scale R

The MSR mass absorbs self-energy corrections coming from scales above R (see **Figure 2** and compare with the $\overline{\rm MS}$ mass). The definition above makes it possible to choose an R that is much smaller than m_t, consistent with the renormalization group. In practical applications, R should be set to the momentum scale that governs the soft quantum fluctuations affecting the mass sensitivity of the observable (e.g., the width of the resonance in the $m_t^{\rm reco}$ distribution). In Equation 8, the second peculiar-looking linear term in R is essential because, in the difference $m_t^0 A^{\rm fin}(m_t^0/R) - RA^{\rm fin}(1)$, all linear sensitivity to soft momenta (in the top resonance frame) cancels, so that the

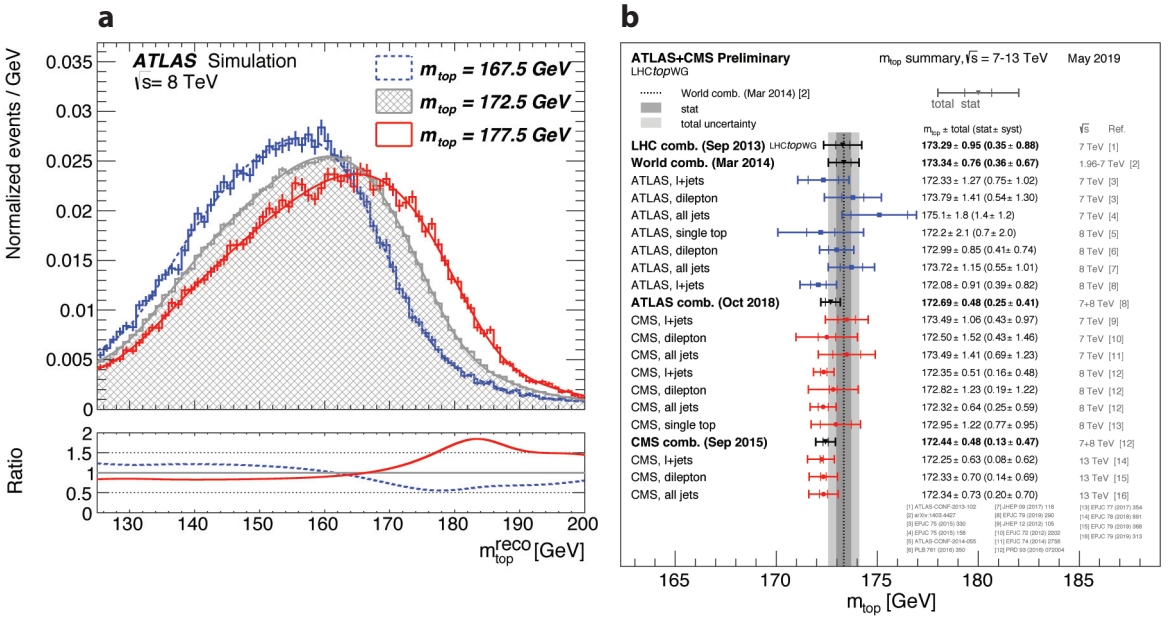

Figure 3

(*a*) Top mass dependence of the reconstructed top invariant mass m_t^{reco} obtained from top decays into three jets from multipurpose Monte Carlo event generator simulations performed by the ATLAS Collaboration. Panel reproduced with permission from Reference 48. (*b*) Collection of recent direct top mass measurements performed at the Large Hadron Collider (LHC). Panel reproduced with permission from the LHC Top Working Group (**https://twiki.cern.ch/twiki/bin/view/LHCPhysics/LHCTopWGSummaryPlots#Top_Quark_Mass**); copyright 2019 CERN for the benefit of the ATLAS and CMS Collaborations/CC BY 4.0.

"bad" soft-momentum contributions in the top self-energy of Equation 4 are still left to cancel in calculations for processes, as was the case for the $\overline{\text{MS}}$ mass $\overline{m}_t(\mu)$. The MSR mass is therefore also a short-distance mass. The trade-off is that the MSR mass has a renormalization group linear equation in R,

$$\frac{\mathrm{d}}{\mathrm{d}\ln R}\, m_t^{\text{MSR}}(R) = -\frac{4}{3}\, R\left(\frac{\alpha_s(R)}{\pi}\right) + \ldots, \qquad 9.$$

which is a generic requirement for a short-distance mass scheme with a renormalization scale $R < m_t$ (52, 53). The MSR mass is prototypical for the class of low-scale short-distance masses devised in the last two decades for quantum field theory calculations for B mesons, heavy quarkonia, and top resonance physics, such as the kinetic (54), 1S (55–57), potential-subtracted (58), RS (59), and jet masses (60). The MSR mass is, however, the only low-scale short-distance mass that is, like the $\overline{\text{MS}}$ mass, defined directly from the quark self-energy diagrams. For $R = \overline{m}_t(\overline{m}_t)$, it differs from the $\overline{\text{MS}}$ mass $\overline{m}_t(\overline{m}_t)$ only by corrections related to two-loop self-energy corrections from virtual top quark loops. Therefore, it can be considered as the natural extension of the $\overline{\text{MS}}$ mass concept for renormalization scales below m_t, as advocated in References 47 and 51. Interestingly, the MSR mass $m_t^{\text{MSR}}(R)$ is also numerically close to the other low-scale short-distance masses at their respective intrinsic scales (see **Figure 4**, which shows $m_t^{\text{MSR}}(R)$ together with the 1S mass and potential-subtracted masses at three representative scales). From a numerical point of view, the $\overline{\text{MS}}$ mass $\overline{m}(\mu)$ and the MSR mass $m_t^{\text{MSR}}(R)$ can be related to each other and to other low-scale short-distance masses with a precision of 30 MeV or better using available results from the

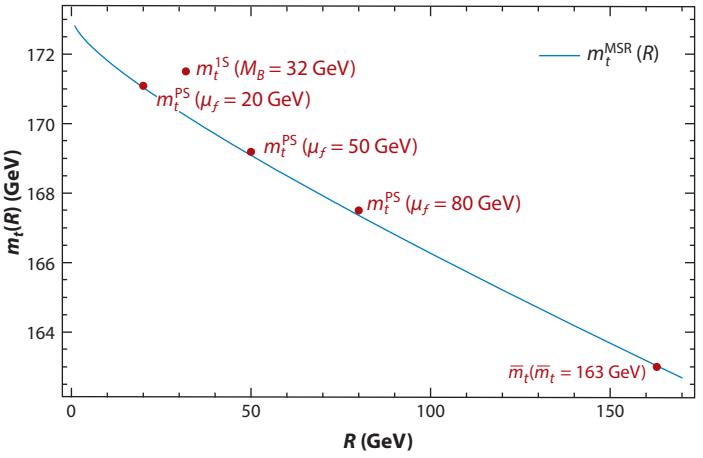

Figure 4

MSR mass $m_t^{\rm MSR}(R)$ over R (*blue line*), 1S mass $m_t^{\rm 1S}$, and potential-subtracted masses $m_t^{\rm PS}(\mu_f)$ for $\mu_f = 20$, 50, and 80 GeV, taking $\overline{m}_t(\overline{m}_t) = 163$ GeV as input. Conversion errors are smaller than the dot sizes. Data from Reference 47.

literature (see, e.g., References 51, 61).[5] This 30-MeV precision represents the principal theoretical limitation of short-distance top mass determinations and is fully adequate for the era of hadron colliders.

The most frequently used top quark mass scheme in perturbative computations is the pole scheme $m_t^{\rm pole}$ (see **Figure 2**), where self-energy corrections from all scales are absorbed into the mass:

$$m_t^{\rm pole} = m_t^0 \left\{1 + \left(\frac{\alpha_s(\mu)}{\pi}\right)\left[\frac{1}{\epsilon} + \ln(4\pi e^{-\gamma_E}) + A^{\rm fin}(m_t^0/\mu)\right]\right\} + \ldots. \qquad 10.$$

By definition, in the pole scheme all perturbative quantum corrections to the pole of the propagator vanish. Thus, $m_t^{\rm pole}$ is the mass of the top quark states that appear in parton-level scattering amplitudes in the approximation where top quarks are treated as real external (or asymptotic) particles (62, 63). Because the mass of the formally defined top quark asymptotic states is renormalization scale invariant, infrared finite, and gauge invariant at the level of perturbation theory (36, 64), it seems to be unique and physical, at least at the parton level. However, as mentioned above, because of the top quark's color charge, this concept is actually unphysical when considering a precision of 0.5 GeV or below. In fact, due to the term $A^{\rm fin}$, the expression on the right-hand side of Equation 10 depends linearly on how infrared momenta are regularized (recall the example of a gluon mass regulator shown in Equation 5). Thus, the pole of the top quark propagator (and the meaning of the mass of a top quark asymptotic state) depends linearly on how infrared momenta (in a top resonance frame) are treated. However, what is commonly called the pole mass $m_t^{\rm pole}$ in the context of QCD is defined strictly within dimensional regularization, where, for instance, the infrared regulator gluon mass term λ shown in Equation 5 does not arise.

The pole mass $m_t^{\rm pole}$ is obtained from the MSR mass $m_t^{\rm MSR}(R)$ taking the formal limit $R \to 0$, so that the MSR mass can be seen as a scheme that formally interpolates between the pole and the

[5] Current uncertainties in the strong coupling do not allow this precision in relating all short-distance masses. From Equations 11 and 12, one can see that an uncertainty in the strong coupling $\alpha_s(M_z)$ of 0.001 results in a parametric uncertainty in the relation between a low-scale short-distance top mass and an $\overline{\rm MS}$ top mass of around 70 MeV.

$\overline{\rm MS}$ masses. For finite R, the relation between the pole and MSR masses reads

$$m_t^{\rm pole} - m_t^{\rm MSR}(R) = \frac{4}{3}\left(\frac{\alpha_s(R)}{\pi}\right) R + \ldots . \qquad 11.$$

In comparison, the relation between the pole and $\overline{\rm MS}$ masses has the form

$$m_t^{\rm pole} - \overline{m}_t(\mu) = \frac{4}{3}\left(\frac{\alpha_s(\mu)}{\pi}\right) \overline{m}_t(\mu) + \ldots . \qquad 12.$$

From the conceptional point of view, the MSR mass $m_t^{\rm MSR}(R)$ can also be seen as a scheme designed for observables where (virtual and real) QCD corrections below the scale R are unresolved so that the self-energy corrections below R, which are not absorbed into $m_t^{\rm MSR}(R)$, are left to cancel with other (real or virtual) quantum fluctuations from scales below R in a top resonance frame. In this context, the pole mass scheme is based on the unphysical view that virtual and real perturbative QCD corrections can be resolved down to arbitrarily small scales.

The unphysical character of the pole mass concept is reflected in the fact that the perturbative series for physical observables in the pole scheme carry the so-called "pole mass renormalon ambiguity" (65–67). At this point, some general aspects of renormalons should be explained because they do not arise only for the pole mass. Renormalons arise in all parton-level cross sections $\hat{\sigma}$ computed in dimensional regularization—even for observables involving only massless quarks or gluons—because the perturbation series for all QCD observables are asymptotic series, as mentioned in Section 2.1. Thus, the terms in the perturbation series may decrease at low orders, but they eventually adopt divergent patterns, which I call "turnover" in the following sections. These divergent patterns in QCD perturbation theory, which were discovered early in the history of QCD (68–70), can be caused by sensitivities to physical infrared QCD dynamical effects that are directly associated with specific types of nonperturbative corrections contained in $\sigma^{\rm NP}$. So, nonperturbative contributions to $\sigma^{\rm NP}$ having characteristic scaling behaviors in powers of $(\Lambda_{\rm QCD}/Q)^n$ have a one-to-one correspondence to specific types of asymptotic divergent patterns (71, 72). This correspondence is well understood mathematically, and the associated divergent patterns of the perturbative coefficients can be quantified analytically to all orders. The generic rule applies that the lower the power of n in a contribution to $\sigma^{\rm NP}$, the stronger the associated asymptotic divergent pattern and the lower the order of turnover. The formal mechanism that brings it all together is as follows: When making predictions for the observable $\sigma^{\rm exp}$, the correction term $\sigma^{\rm NP}$ compensates, order-by-order in perturbation theory, for the divergent patterns in $\hat{\sigma}$ and at the same time adds the corresponding physical nonperturbative corrections. This connection is a fundamental aspect of QCD predictions of the form shown in Equation 3, in which perturbative and nonperturbative contributions are separated and dimensional regularization is used to regulate infrared momenta (71, 72). In practice, it may not be easy to realize this mechanism at high perturbative order, but for most applications the available perturbative corrections seem to be below the order of turnover.

When making parton-level predictions in the pole mass scheme, there is a renormalon that arises from a divergent pattern coming from the virtual nonself-energy corrections that are soft (in a top resonance frame) and left uncanceled, as mentioned several times above. The divergent pattern of this pole mass renormalon has the same mathematical structure as those patterns related to contributions to $\sigma^{\rm NP}$ that are linear in $\Lambda_{\rm QCD}$, in one-to-one correspondence to the linear infrared sensitivity of $A^{\rm fin}$ (see Equation 5). As such, the pole mass renormalon is rather strong, and its numerical impact and even the turnover point can be visible and relevant already at the low orders accessible to perturbative calculations. Thus, the pole mass renormalon looks very much like an uncertainty due to some missing physical nonperturbative information to be remedied by

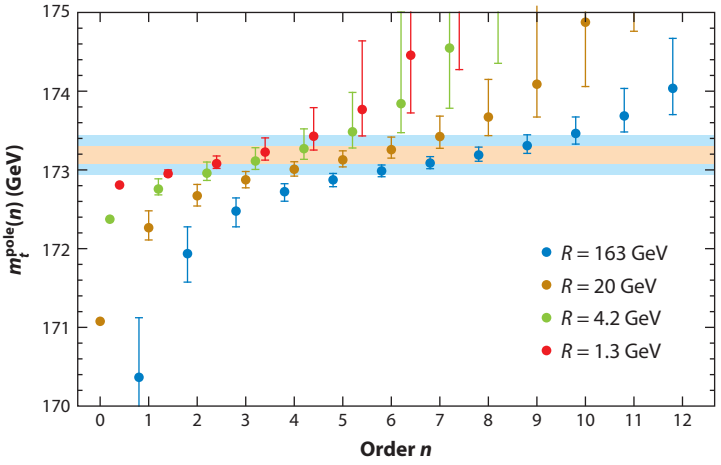

Figure 5

Pole mass determinations as a function of order n from $m_t^{\text{MSR}}(R)$ for $R = 163$, 20, 4.2, and 1.3 GeV using the series shown in Equation 11, which is known to all orders. The values of $m_t^{\text{MSR}}(R)$, shown as the dots at order $n = 0$, are determined from $\overline{m}_t(\overline{m}_t) = 163$ GeV using matching at $R = \overline{m}_t(\overline{m}_t) = 163$ GeV and the R-evolution equation (Equation 9) at four loops and finite bottom and charm masses with $\overline{m}_b(\overline{m}_b) = 4.2$ GeV and $\overline{m}_c(\overline{m}_c) = 1.3$ GeV. The error bars arise from renormalization scale variations. Data from Reference 47. The orange band represents the best estimate for the pole mass including the renormalon ambiguity estimated in Reference 75, and the blue band indicates the one obtained in Reference 47.

a contribution to σ^{NP} that is linear in Λ_{QCD} [i.e., proportional to $\Lambda_{\text{QCD}}(\text{d}/\text{d}m_t)\hat{\sigma}$]. However, this view is incorrect because the pole mass renormalon pattern is an artificial problem tied to the unphysical concept of a top quark particle pole and not related to a physical effect (which would be encoded in σ^{NP} in Equation 3) (65–67). Using instead a short-distance mass at an appropriate renormalization scale, this renormalon just does not arise. If the pole mass must be used, it is necessary to truncate at the order at which the correction is minimal—that is, around the order of turnover. The inability to do so in a unique way in practice (and even in principle) results in an ambiguity in the determination of m_t^{pole}, which is called the pole mass renormalon ambiguity. The ambiguity is unchanged even if the top quark's finite lifetime is accounted for, which shifts the top quark propagator pole to a complex p^2 value (73). This fact underlines the unphysical character of the pole mass renormalon.

The divergent pattern of the pole mass renormalon happens to grow so rapidly with order that for many quantities, the explicitly calculated coefficients are already completely saturated by it (47, 51, 74, 75).[6] The ambiguity is also reflected in the form of Equation 11, where the limit $R \to 0$ apparently can be taken only by crossing the Landau pole in $\alpha_s(R)$. Since this would generate a nonperturbative contribution to the pole mass (which is unphysical), the limit $R \to 0$ is taken keeping the scale μ in $\alpha_s(\mu)$ finite. This is another way to understand how the divergence pattern in the coefficients of perturbative series in the pole mass scheme arises. The pattern is illustrated in **Figure 5**, which shows pole masses determined from the MSR mass $m_t^{\text{MSR}}(R)$ at different values of R from Equation 11 as a function of truncation order n. For

[6]The series for $m_t^{\text{pole}} - m_t^{\text{MSR}}(R)$ and $m_t^{\text{pole}} - \overline{m}_t(\mu)$ in Equations 11 and 12, respectively, have been computed explicitly up to $\mathcal{O}(\alpha_s^4)$ (36–41). The large-order renormalon asymptotics of the pole mass renormalon has been shown to saturate the $\mathcal{O}(\alpha_s^3)$ and $\mathcal{O}(\alpha_s^4)$ coefficients, and the coefficients at $\mathcal{O}(\alpha_s^n)$ for $n > 4$ are therefore known with a precision of a few percent from their asymptotic behavior (51, 75).

the orders $n > 4$, the asymptotic estimates are used (see Footnote 5). The observed pattern is representative of the behavior of pole mass determinations from physical observables (not affected linearly by other kinds of soft QCD effects) where the mass dependence is governed by QCD dynamics at the scale R. For $R \gtrsim m_t$ (relevant for total inclusive cross sections; see the results for $R = 163$ GeV), the order of turnover is seven or eight, and one needs to go for many orders to get to the range of the best estimate for m_t^{pole}. For $R \lesssim 10$ GeV (relevant for some differential cross sections with kinematic top mass sensitivity), the order of turnover is two or three. Here one can reach the range of the best estimate for m_t^{pole} already at orders accessible with available perturbative computations (see Section 3.1), and even the tree-level results are close to it.[7] The size of the ambiguity and final range for the best estimate for m_t^{pole} (around the order of turnover) can be formally proven to be independent of R, and the size of the ambiguity can be formally shown to be of order Λ_{QCD} (65–67). Recent analyses have quantified it as 110 MeV (75) and 250 MeV (47) (width of the horizontal bands in **Figure 5**) using all available theoretical information.[8] **Figure 5** also underscores that when numerically converting between pole mass and short-distance mass values, it is essential to truncate at the respective order of turnover, which may differ from the perturbative order used in the calculation. I adopt the approach from Reference 47 when quoting numerical values for the difference between m_t^{pole} and short-distance masses.

It should be stressed, however, that even when a short-distance mass scheme is used for a parton-level top mass–dependent cross section $\hat{\sigma}$, one still has to deal with possible contributions to σ^{NP}, and in particular with those that depend linearly on Λ_{QCD}, which also affect mass determinations in a linear way. Such linear nonperturbative effects are unavoidable for LHC observables because the hard processes generating the top mass sensitivity always involve top states (e.g., single top, $t\bar{t}$) in a nonsinglet color configuration or depend on jets. For these observables, the description of the physically observable top mass dependence always involves nonperturbative color neutralization processes that enter σ^{NP} linearly, as emphasized at the end of Section 2.1. For top mass determinations, these nonperturbative color neutralization processes must be understood separately and disentangled from the top mass dependence to reach the best possible theoretical uncertainty limit of 30 MeV for a short-distance mass determination as mentioned above.[9] The limit can be approached for e^+e^- colliders (see Footnote 3), but it is very difficult to do so for LHC observables. However, the size of the physical color neutralization corrections at the LHC is observable-dependent and in some cases can be small or can be controlled field-theoretically using QCD factorization; for related studies, readers are referred to References 77 and 78, respectively.

[7]This example also illustrates that in perturbative computations for observables where R is large, it is more natural to use $m_t^{\text{MSR}}(R)$ (for $R < m_t$) or $\overline{m}_t(R)$ (for $R > m_t$) as a mass scheme, whereas m_t^{pole} or $m_t^{\text{MSR}}(R)$ is more natural for observables where R is small.

[8]These estimates were obtained for finite charm and bottom quark masses. For $m_c = m_b = 0$, the ambiguity was estimated as 70 MeV in Reference 75 and as 180 MeV in Reference 47. The dependence on the charm and bottom masses reflects the strong sensitivity of the pole mass on small momenta. It arises because the ambiguity is dependent on the leading β-function coefficient of the strong coupling α_s, which increases when the number of massless quarks decreases.

[9]There is the possibility of a partial cancellation between the pole mass renormalon divergent pattern and the renormalon pattern related to a mass-unrelated physical linear nonperturbative effect due to a sign difference in the associated divergent patterns in the perturbative series. Examples for such observables have been discussed in, for instance, References 24, 76, and 77, and it was demonstrated in References 24 and 76 that the respective renormalon patterns arise from different dynamical modes located in separated and factorizable physical phase space regions. I disagree with the argument made in Reference 77 that in such a case the attainable precision of a pole mass determination is higher than for a short-distance mass determination.

NNLO: next-to-next-to-leading-order approximation in fixed-order perturbation theory

NNLL: next-to-next-to-leading-order approximation in logarithm-resummed perturbation theory

NWA: narrow-width approximation

LO: leading (lowest)-order approximation in fixed-order perturbation theory

3. STATUS OF TOP MASS DETERMINATIONS AT THE LHC

In this section, I discuss the status of state-of-the-art top mass determinations and focus on the experimental methods and theoretical tools employed in the analyses. Because there are already many excellent reviews on the experimental aspects of the measurements (1, 14, 79, 80), on projections for the HL-LHC (see 2, 81, and references therein), and on the status of the employed Monte Carlo tools (1, 82), I refrain from a detailed technical presentation and instead concentrate on the critical conceptual aspects of top mass measurements at the LHC.

3.1. Fixed-Order Calculations

State-of-the-art fixed-order parton-level computations—that is, perturbation series for $\hat{\sigma}$ as expansions in powers of α_s—have reached a high level of sophistication and are primarily based on numerical methods. For the production of on-shell top quark pairs, QCD corrections at next-to-next-to-leading order (NNLO) (83) are available, including the resummation of QCD next-to-next-to-leading logarithms (NNLLs) involving the ratio of the top quark transverse momentum to the top mass (p_T/m_t) (84) and also accounting for NLO electroweak corrections (85). In the narrow-width approximation (NWA) for the top quark, NNLO QCD calculations for on-shell top quark production and top quark decay (86) have been combined to allow for fully differential predictions (87). These results neglect finite-lifetime effects and do not account for the summation of large logarithms of the ratio Γ_t/m_t related to the top quark's low-energy off-shell dynamics. Finite-lifetime effects have been included in fixed-order QCD NLO computations for the $W^+W^-b\bar{b}$ final state, including W decays in leptons (88) and jets (89). These calculations describe top production, top decay to $W^+W^-b\bar{b}$ final states, and $W^+W^-b\bar{b}$ nonresonant production. The latter results are less precise concerning QCD corrections and lack the resummation of logarithmic terms. NLO and higher fixed-order calculations provide reliable approximations with controlled top mass scheme dependence to $\hat{\sigma}$ for observables where the typical momenta of the QCD dynamics governing the mass dependence are of the size m_t or larger. Relevant to top mass measurements, these observables include the total inclusive $t\bar{t}$ cross section, the $t\bar{t}$ + jet invariant mass $M_{t\bar{t}j}$ for values much larger than $2m_t$, and leptonic distributions away from kinematic threshold structures (kinks, shoulders, endpoints). Including the summation of logarithms of the ratio p_T/m_t further provides reliable parton-level descriptions of the p_T and the $t\bar{t}$ invariant mass $M_{t\bar{t}}$ distributions in the boosted top region where $p_T \gg m_t$ or $M_{t\bar{t}} \gg 2m_t$. Interestingly, almost all fixed-order calculations are available only in the pole mass scheme. Making parton-level predictions in short-distance top mass schemes requires a re-expansion of the perturbative series using Equation 11 and/or Equation 12 and the computation of mass derivatives. Reference 90 provides a dedicated calculation of the total inclusive $t\bar{t}$ cross section at NNLO in the $\overline{\text{MS}}$ top mass scheme.

3.2. Multipurpose Monte Carlo Event Generators

MMCs (91–93) form the backbone of essentially all experimental analyses at the LHC. They are used to simulate all processes spanning from the collision of protons to the emergence of the observable hadrons. MMCs also are used to design novel observables and measurements, for detector simulations, and to determine efficiencies and acceptances. As illustrated in **Figure 6**, they combine the quark and gluon (parton) structure of the colliding protons (big gray blobs), tree-level leading-order (LO) matrix elements for the hard parton interactions (red lines and blob), a PS that describes the branching of the hard partons into lower-energy partons (dark blue straight and curly lines), and a hadronization model. The hadronization model turns the high-multiplicity

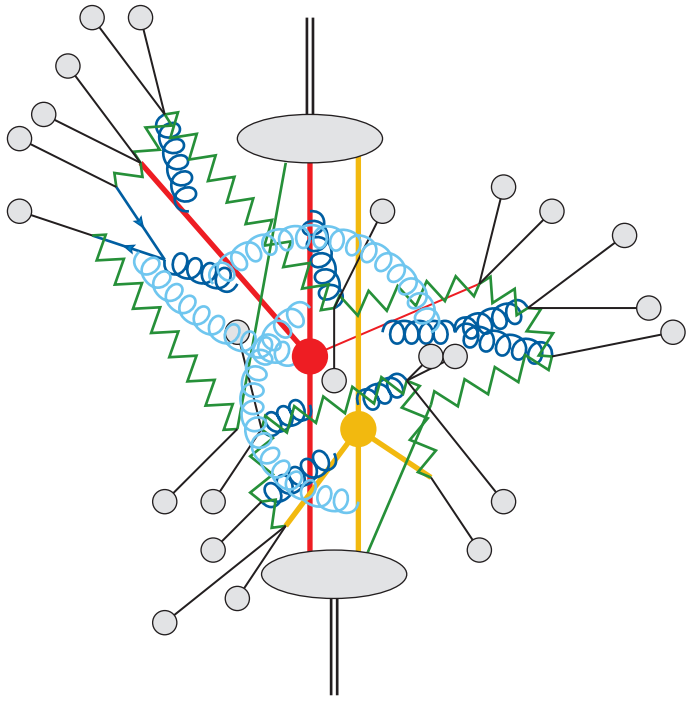

Figure 6

Generic illustration of the components of multipurpose Monte Carlo event generators: quark and gluon (parton) structure functions of the colliding protons (*big gray blobs*), tree-level leading-order matrix elements for the hard parton interactions (*red lines* and *blob*), the parton shower (*dark blue straight* and *curly lines*), the hadronization model (*small gray blobs* and *green zigzag lines*), multiparton interactions (*yellow lines* and *blob*), and color reconnection effects (*light blue curly lines*).

partonic states that emerge after the PS terminates into the observable hadronic particles, accounting for the color flow in the large-N_c limit (small gray blobs for hadrons and green zigzag lines for color correlations). State-of-the-art MMCs also provide descriptions of multiparton interactions (yellow lines and blob) and color reconnection effects (light blue curly lines). The hard matrix elements and the PS provide descriptions of $\hat{\sigma}$ in the collinear and soft limits, where fixed-order calculations are insufficient because of large logarithmic terms. These descriptions can be NLL precise for certain simple classes of observables (e.g., event shapes) but in general are less precise even though they can still provide an adequate description for experimental simulations (94, 95). State-of-the art PSs are based either on angular-ordered coherent branching (CB) (96) [as used by default in the Herwig (91) MMC family] or on transverse-momentum-ordered dipole showering (97) [as used in the Pythia (92) and Sherpa (93) MMCs and optionally in Herwig (98)]. Differences between the two PS types arise, for example, in the treatment of nonglobal observables, where CB has intrinsic restrictions, or in momentum recoil effects, where dipole showering is based on a local treatment for each parton branching, leading to precision issues for global observables. The description of the proton structure in terms of parton distribution function and the hadronization models provides approximate descriptions for σ^{NP}. The hadronization models are based on the concepts of decaying clusters (99) and the breaking of QCD strings (100). Their parameters are fixed not from first principles QCD but, rather, through the tuning procedure—that is, by demanding that the MMCs reproduce a certain set of experimental differential reference

CB: coherent branching

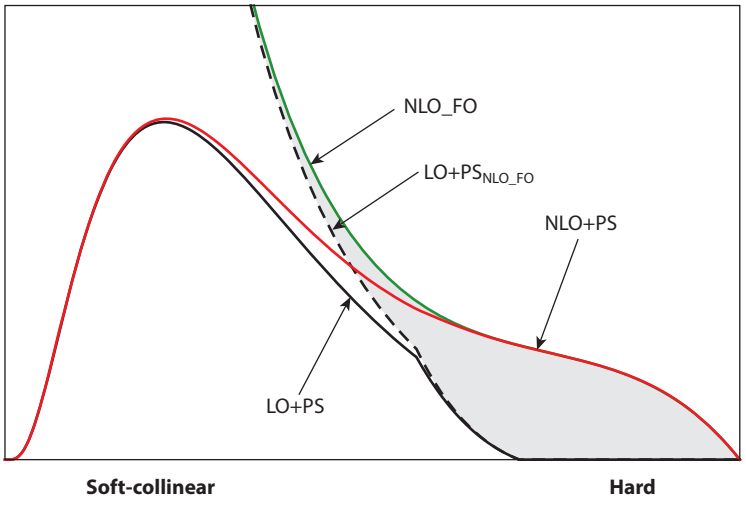

Figure 7

Generic structure of a kinematic distribution with a top mass–sensitive kinematic threshold structure in the soft-collinear region (*left side*) obtained by NLO-matched MMCs (NLO+PS, *red line*) and unmatched MMCs (LO+PS, *solid black line*). The distribution at NLO in QCD fixed-order perturbation theory (NLO_FO, *green line*) is singular and diverges in the soft-collinear limit. The PS evolution of the unmatched MMCs sums the leading logarithmic singular terms to all orders in fixed-order perturbation theory, leading to a physically meaningful approximation with Sudakov suppression in the soft-collinear limit (LO+PS, *solid black line*). The matching procedure adds the difference between unmatched MMC description expanded out to NLO (LO+PS$_{NLO_FO}$, *dashed black line*) and the NLO QCD fixed-order (NLO_FO, *green line*) results, both of which are singular, to the tail of the unmatched MMC distribution in the region dominated by hard radiation events (*gray area*, *right-hand side*). Since at the NLO fixed-order level the first hard emission arises from the first emission generated by the PS, the matching procedure elevates the first hard PS emission of the NLO-matched MMCs (NLO+PS, *red line*) to full NLO precision in QCD. Some distributions have tails on both sides of the soft-collinear region. Abbreviations: FO, fixed order; LO, leading order; MMC, multipurpose Monte Carlo event generator; NLO, next-to-leading order; PS, parton shower; QCD, quantum chromodynamics.

cross sections. Thus, the MMCs can provide adequate descriptions even when the PS description is less precise.

The precision of PSs in MMCs can be elevated by matching them with NLO matrix elements (referred to as NLO+PS). Matched generators such as MacGraph5_aMC@NLO (101, 102) or the POWHEG (103) procedure and related methods available in Herwig (104) and Sherpa (105) improve the description of the first hard PS emission to NLO precision (typically with transverse momenta larger than 10 GeV) but leave the soft and collinear emissions and hadronization provided by the underlying Monte Carlo event generators unchanged. **Figure 7** illustrates generically how the matching affects the distribution of a top mass–sensitive kinematic distribution. MMCs share, in an observable-dependent way, the aspects of first principles calculations as well as model descriptions, the primary goal of which is the adequate description of experimentally observable quantities. Obtaining reliable estimates of the theoretical uncertainties of the MMC descriptions is therefore a nontrivial task. There is an ongoing effort to improve the theoretical basis of MMCs and the methods to estimate their uncertainties for observable quantities (see, e.g., 94, 106–108).

NLO+PS: next-to-leading order–matched parton shower

For top quark physics, the Pythia (92) and Herwig (91, 109) event generators are most often employed. It is an essential aspect of all experimental top quark measurements to properly estimate the theoretical or model uncertainties of the MMC descriptions. The common approach of

the experimental collaborations is to analyze the variations obtained from a few different MMC implementations that are considered reasonable. Limitations of state-of-the-art MMCs that are particularly relevant for LHC top mass measurements concern subtle issues such as color reconnection (110–114), multiparticle interactions (115, 116), the precise determination of parameters of the hadronization models (117), and finite-lifetime effects (118, 119). In addition, MMCs used for state-of-the-art LHC analyses only contain LO matrix elements for the top decay. A serious limitation in principle is that all massive quark PSs are theoretically based on the quasi-collinear (i.e., boosted top) approximation, while most top mass measurements rely on top events with relatively low top quark transverse momenta p_T of around 100 GeV and velocities v_t of about 0.5. How this restriction affects current top mass measurements is, to the best of my knowledge, unknown. Furthermore, the parton-level descriptions of top mass–sensitive kinematic threshold structures provided by NLO-matched MMCs are not elevated to subleading QCD precision because sharp threshold structures are governed by soft and collinear radiation and hadronization effects. Examples of observables subject to this issue are all kinematic observables reconstructed from a single top quark, such as its reconstructed invariant mass m_t^{reco}, or kinematic endpoint regions for variables such as the lepton energy E_ℓ or the lepton and b jet invariant mass $M_{b\ell}$. Also, the reconstructed $t\bar{t}$ invariant mass $M_{t\bar{t}}$ in the threshold region where $M_{t\bar{t}} \approx 2m_t$ is subject to this issue because of soft radiation effects related to the $t\bar{t}$ pair produced with small relative velocity in a color-octet state, Coulomb binding corrections, and coherence effects in the simultaneous weak decay of the $t\bar{t}$ pair. I reiterate that observables with such threshold structures are responsible for the high top mass sensitivity of the direct mass measurements. However, it also should be mentioned that NLO-matched MMCs can provide NLO reliable parton-level approximations for observables $\hat{\sigma}$ where the top mass sensitivity is generated exclusively by hard interactions (referred to in Section 2.2 as observables with indirect top mass sensitivity; see text below Equation 7). Examples are the total cross section and the mass variables $M_{t\bar{t}}$ and $M_{t\bar{t}j}$ far above the threshold. So, if the NLO-matching procedure uses the identification $m_t^{\text{MC}} = m_t^{\text{pole}}$, a measurement of m_t^{MC} from such hard-interaction-dominated observables can indeed be considered as a pole mass measurement.

In this context, measurements of the top quark mass are more subtle than measurements of physical observables (e.g., hadron and lepton momenta, lifetimes, hadronic and jet cross sections) because the top mass and its couplings are not physical observables but, rather, theoretically defined Lagrangian parameters. For their measurement, the MMC employed has to provide perturbative ($\hat{\sigma}$) and nonperturbative (σ^{NP}) descriptions that are separately consistent with QCD, such that the mass and coupling parameters of the generator retain a definite and observable-independent relation to the QCD Lagrangian parameters. This relation is diluted or even lost to the extent that the tuning compensates for conceptual deficiencies of the PS regardless of whether the MMC describes the data well. This issue is particularly subtle for the top quark mass parameter m_t^{MC} because the MMC has to reliably simulate all color neutralization (linear in Λ_{QCD}) and finite-lifetime (linear in Γ_t) effects consistent with the SM. This issue is at the core of the MMC top mass interpretation problem related to the direct top mass measurements. Only limited quantitative knowledge regarding this complex set of issues exists to date.

3.3. Experimental Analyses

The direct measurements are the most precise top quark mass extractions carried out at the LHC. They are based on kinematic observables constructed from reconstructed top decay products (light quark and b quark jets, leptons) for the different accessible top decay (semileptonic or hadronic) and top production modes ($t\bar{t}$ and single top events). For the template method, the b jet lepton

invariant mass $M_{\ell b}$ (dilepton $t\bar{t}$ and single top events) and reconstructed top invariant mass m_t^{reco} (see **Figure 3*a***) distributions are used. For the ideogram and matrix element methods, the likelihood of a whole reconstructed final state being compatible with a $t\bar{t}$ production hypothesis is determined event-by-event. Both approaches rely fully on the PS and hadronization components of MMCs for the theoretical description; thus, the mass parameter m_t^{MC} is extracted from the best fits or the highest cumulative likelihood. **Figure 3*b*** provides a summary of all state-of-the-art direct top mass measurements. The current world average quotes $m_t^{\text{MC}} = 172.9 \pm 0.4$ GeV (1). The latest CMS and ATLAS combinations have yielded $m_t^{\text{MC}} = 172.26 \pm 0.61$ GeV (120) (for a measurement using single top events, see Reference 121) and $m_t^{\text{MC}} = 172.69 \pm 0.48$ GeV (48), respectively. It should be noted that the final Tevatron combination obtained $m_t^{\text{MC}} = 174.34 \pm 0.64$ GeV (122).[10] As mentioned above, the $M_{\ell b}$ and m_t^{reco} variables employed for the template method are examples of observables whose MMC description is not improved by the NLO matching. The ideogram and matrix element methods are based on observables of the same kind because such observables have the highest mass sensitivity for the reconstructed decay products. Significant work has been invested in the determination of the systematic uncertainties by the ATLAS and CMS Collaborations. These efforts, however, do not provide insights concerning the interpretation problem of m_t^{MC}, which—as long as the issue is unresolved—must be viewed as an additional systematic error in the relation of m_t^{MC} to a top mass scheme defined in field theory.

So-called pole mass measurements are based on the inclusive and differential $t\bar{t}$ cross sections, for which theoretical parton-level predictions expressed in the pole mass scheme from NNLO+NNLL calculations for the total cross section $\sigma(t\bar{t} + X)$ (125) are available, and NLO-matched Monte Carlo event generators for the reconstructed $t\bar{t}$ + jet invariant mass $M_{t\bar{t}j}$ (126), (di)leptonic variables (127), and $t\bar{t}$ invariant mass $M_{t\bar{t}}$ can be employed. A summary of these measurements is shown in **Figure 8*b***, and the current world average quotes $m_t^{\text{pole}} = 173.1 \pm 0.9$ GeV (1). The inclusive $t\bar{t}$ cross section and the invariant masses $M_{t\bar{t}}$ and $M_{t\bar{t}j}$ (away from the lower threshold at $2m_t$) are examples of observables where the top mass sensitivity is indirect (i.e., exclusively tied to hard interactions). For these observables, parton-level predictions at NLO (or higher) and NLO-matched Monte Carlo event generators carry NLO information on the mass scheme. Furthermore, for these observables the resolution scale R for the QCD dynamics governing the mass sensitivity (see **Figure 5**) is of order or larger than m_t. One can therefore expect that the theoretical errors of the parton-level prediction may be further reduced when even higher-order fixed-order or resummed calculations become available or when the $\overline{\text{MS}}$ top mass scheme is employed. Inclusive cross-section measurements yielded $m_t^{\text{pole}} = 172.9^{+2.5}_{-2.6}$ GeV [ATLAS; 7- and 8-TeV data (128)], $m_t^{\text{pole}} = 173.8^{+1.7}_{-1.8}$ GeV [CMS; 7- and 8-TeV data (129)], and $m_t^{\text{pole}} = 169.9^{+2.0}_{-2.2}$ GeV [CMS; 13-TeV data (130)].[11] The relatively larger errors compared with those from the direct measurements result from the uncertainty in the normalization of the inclusive cross section (dominated by gluon luminosity uncertainties and renormalization scale variation in the cross-section fixed-order calculations) and its relatively weaker dependence

[10] Much could likely be learned from knowing the reasons for the discrepancy between the Tevatron and the LHC measurements. The impact of a recalibration of the jet energy scale for the Tevatron D0 lepton + jet direct mass measurement (123) was analyzed in Reference 124.

[11] The analysis of Reference 130 also studied the strong correlations among the extracted top mass, the value of the strong coupling $\alpha_s(M_Z)$, and the employed set of parton distribution functions (131–134). The quoted lower value for m^{pole} is based on a set of parton distribution functions (131) that is determined in a simultaneous fit with α_s. The associated range of α_s values is below that of the world average. The analysis also determined the $\overline{\text{MS}}$ top mass $\overline{m}_t(\overline{m}_t)$ based on the calculations of Reference 90.

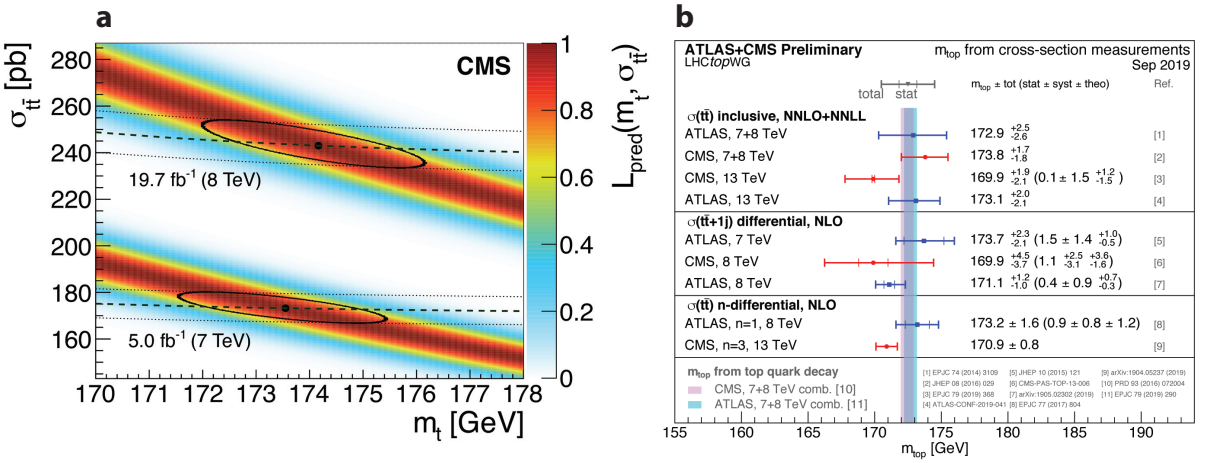

Figure 8

(*a*) Top mass dependence of the measured (*black dashed* and *dotted lines*) and theoretical predicted (*dark shaded band*) inclusive $t\bar{t}$ cross section and the resulting best m_t^{pole} fit range obtained by the CMS Collaboration on the basis of LHC 7- and 8-TeV data. Panel reproduced with permission from Reference 129. (*b*) Summary of recent pole mass measurements. Panel reproduced with permission from the LHC Top Working Group (**https://twiki.cern.ch/twiki/bin/view/LHCPhysics/LHCTopWGSummaryPlots#Top_Quark_Mass**); copyright 2019 CERN for the benefit of the ATLAS and CMS Collaborations/CC BY 4.0. Abbreviations: LHC, Large Hadron Collider; NLO, next-to-leading order; NNLL, next-to-next-to-leading logarithm; NNLO, next-to-next-to-leading order.

on m_t (see **Figure 8*a***). A recent $M_{t\bar{t}j}$ measurement by the ATLAS Collaboration yielded $m_t^{\text{pole}} = 171.1^{+1.2}_{-1.1}$ GeV (135), which is more precise because the distribution exhibits a mass-sensitive broad hump. A measurement using leptonic distributions by the ATLAS Collaboration obtained $m_t^{\text{pole}} = 173.2 \pm 1.6$ GeV (136). It should be pointed out that for leptonic distributions, the color neutralization effects mentioned above indirectly affect the momentum of the decaying W boson and cannot be avoided. A CMS analysis including the total inclusive cross section, the $M_{t\bar{t}}$ and the top pair rapidity $y_{t\bar{t}}$ distributions, and a simultaneous α_s and gluon distribution fit obtained $m_t^{\text{pole}} = 170.5 \pm 0.8$ GeV (137)—a finding that poses some tension with the pole mass world average mentioned above. For this CMS analysis, it should be noted that the smaller error compared with that from the inclusive cross-section measurements mentioned above partly results from the inclusion of the $M_{t\bar{t}}$ distribution, which is kinematically sensitive to the top mass in the threshold region $M_{t\bar{t}} \approx 2m_t$. This issue should be examined thoroughly to ensure reliable theoretical descriptions because the theoretical fixed-order calculations employed for the analysis to determine the top mass are based on an approximation in which $M_{t\bar{t}}$ is defined from the sum of the four-momenta of an on-shell top and antitop quark. Furthermore, NLO-matched MMC descriptions, which are used to relate the reconstructed observable $M_{t\bar{t}}$ distribution to the theory calculation, do not have subleading QCD precision for $M_{t\bar{t}}$ in the threshold region, and many of the $t\bar{t}$ pairs are produced in color-octet configurations, for which the effects of soft QCD radiation are significant.

A number of alternative methods to measure m_t have been proposed; these methods are based on differential cross sections with respect to alternative mass-sensitive variables constructed from top decay products. The observables include the M_{T2} variable and variants of it (138, 139), the shape of b jet and B meson energy distributions (140), the J/ψ and lepton invariant mass (141, 142), and secondary vertices from b quark fragmentation (142). They are also motivated by the kinematic properties of a decaying top particle. These observables are affected by issues similar to the direct measurements, albeit with differing systematics and leading to larger uncertainties.

They can also be seen as $m_t^{\rm MC}$ measurements and are consistent with the direct measurements. Because the sensitivity to soft and nonperturbative dynamics can be reduced by jet grooming techniques (143–146), it was, as an alternative, suggested to use the mass of a fat and groomed boosted top quark jet, for which factorized QCD predictions with field-theoretic control of the top mass scheme and nonperturbative effects can be determined (78). In Reference 147, the $\gamma\gamma$ invariant mass spectrum $M_{\gamma\gamma}$ was suggested as a top mass–sensitive variable because it shows a glitch due to large QCD phases and Coulomb bound-state effects when $M_{\gamma\gamma} \approx 2m_t$. In principle, predictions of the $\gamma\gamma$ mass observable allow systematic control of the top mass scheme, but it should be reiterated that the LHC produces significant amounts of $t\bar{t}$ pairs in a color-octet state. Because of the effects of radiation that is soft in the $t\bar{t}$ center-of-mass as well as the lab frame, precise and reliable predictions of $M_{\gamma\gamma}$ are significantly more involved than for the analog $t\bar{t}$ threshold cross section in e^+e^- annihilation (29, 30) and have not been achieved to date. Furthermore, the $\gamma\gamma$ mass method requires the HL-LHC to be competitive in precision with the current pole mass measurement uncertainties.

Overall, current direct and pole mass measurements show good mutual agreement, but the discriminating power of the pole mass measurements is somewhat lower. One can expect that the theoretical uncertainties of pole mass measurements may be further reduced when the corresponding next-higher-order perturbative calculations or improved theoretical approaches become available. An additional reduction of theoretical uncertainties may be achieved when, instead of the pole mass scheme, appropriate scale-dependent short-distance mass schemes such as $\overline{\rm MS}$ or MSR are employed. The use of such schemes should, however, also be accompanied by a substantially increased understanding of a number of systematic effects influencing the size and shape of the related differential cross sections, which currently affect these top mass measurements at the level of 1 GeV or larger. It requires dedicated work for the pole mass measurements to approach the numerical precision of the direct measurements quoted by the ATLAS and CMS Collaborations. However, one should keep in mind that the direct measurements suffer from an additional uncertainty related to the $m_t^{\rm MC}$ interpretation problem.

4. THE CONTROVERSY

The controversy described in Section 1 concerns whether the interpretation problem of $m_t^{\rm MC}$ is large compared with the experimental uncertainties quoted for the direct top mass measurements. The arguments for the two viewpoints can be paraphrased in a concrete form as follows.

There has been the view, advocated in References 148 and 149, to write

$$m_t^{\rm MC} = m_t^{\rm pole} + \Delta_{m_t}^{\rm MC}, \qquad 13.$$

where it is assumed that the identification of the MMC top mass parameter with the pole mass is appropriate to very good approximation and that the term $\Delta_{m_t}^{\rm MC}$ is related to the approximate MMC theory description and modeling. The term $\Delta_{m_t}^{\rm MC}$ is an uncertainty in addition to the uncertainties quoted by the experimental collaborations, but it is argued to be much smaller than those such that it is appropriate to identify $m_t^{\rm MC} = m_t^{\rm pole}$. This view is based on the following argumentation: First, the parton-level components of MMCs (hard matrix elements, PSs) are good approximations to perturbative computations made in the pole scheme. Second, PSs can be assumed to provide a good approximation of soft and collinear perturbative radiation at, in principle, all soft scales for the observables entering the direct measurements. Because self-energy corrections (which are virtual) do not show up explicitly in PSs, they are effectively absorbed into the quark mass parameter $m_t^{\rm MC}$, which would result in this parameter's identification with the pole mass.

The pole mass renormalon ambiguity is argued to be relevant in the sense that the identification of m_t^{MC} with the pole mass breaks down only when experimental uncertainties approach the size of the pole mass ambiguity (which means that the difference $m_t^{\mathrm{MC}} - m_t^{\mathrm{pole}}$ is limited in size by the ambiguity). This breakdown, however, using (for instance) the estimate of 110 MeV for the pole mass ambiguity from Reference 75, does not happen for the current top mass measurements and the projections for the HL-LHC.

Q_0: low-energy cutoff scale of the parton shower evolution

The other view, advocated in References 12 and 18, is to write

$$m_t^{\mathrm{MC},Q_0} = m_t^{\mathrm{MSR}}(R_0) + \Delta_{m_t}^{\mathrm{MC}}(R_0, Q_0), \qquad 14.$$

where R_0 is an appropriate scale. The argumentation is as follows: In state-of-the-art MMCs, the PS evolution terminates at a scale Q_0 around 1 GeV (called the shower cut), which keeps the strong coupling governing the PS in the perturbative regime and prevents the number of partons from becoming too large and computationally unmanageable. Because the PS in MMCs is an approximation of perturbative soft and collinear radiation for scales above Q_0, all (real and virtual) radiation at scales below Q_0 is treated as unresolved and is thus left to combine and cancel. Therefore, the self-energy corrections from scales below Q_0 are not absorbed into m_t^{MC}. This mechanism implies that the generator mass depends on the shower cut Q_0 (and also, in principle, the type of the PS) and is close to the MSR mass $m_t^{\mathrm{MSR}}(R_0)$ for $R_0 \propto Q_0$. Thus, m_t^{MC,Q_0} is a short-distance mass like the MSR mass. The relation can be computed if Q_0 is treated as a factorization scale such that the PS is used only in the perturbative regime and not to model nonperturbative effects (as it should be for a first principles perturbative calculation). Thus, $\Delta_{m_t}^{\mathrm{MC}}(R_0 \propto Q_0, Q_0)$ is a finite, perturbatively computable term scaling like $\alpha_s(Q_0) \times Q_0 \sim 0.5$ GeV. It is not captured by the uncertainties quoted by the experimental collaborations and may not be smaller than them. To determine $\Delta_{m_t}^{\mathrm{MC}}(R_0, Q_0)$ reliably, detailed additional insights into the perturbative precision and structure of PSs and the physical meaning of their shower cut Q_0 are mandatory. A greater level of scrutiny is also needed regarding the theoretical precision of PSs and hadronization models in state-of-the-art MMCs to determine whether $\Delta_{m_t}^{\mathrm{MC}}(R_0, Q_0)$ is observable independently or has a nonperturbative contribution. The size of the pole mass renormalon ambiguity plays no role in Equation 14 because both m_t^{MC,Q_0} and m_t^{MSR} are short-distance masses.

The second view is conceptually more involved than the first. The controversy thus boils down to different judgments on (*a*) whether the first view regarding the smallness of $\Delta_{m_t}^{\mathrm{MC}}$ in Equation 13 indeed applies or whether the formulation of Equation 14 is required[12] and (*b*) whether the impact of the shower cut on the perturbative components of the MMCs is negligible, such that Q_0 is merely a parameter of the hadronization model, or whether Q_0 is an infrared factorization scale at the interface between the perturbative and nonperturbative components of the MMCs that can (and must) be quantified analytically. It should be stressed that even though there is a controversy, given that Q_0 is a relatively small scale of around 1 GeV, we are talking about differences and effects at the level of 0.5 to 1 GeV, but not more than that. In the context of QCD, concerns that m_t^{MC} may be close to the $\overline{\mathrm{MS}}$ mass $\overline{m}_t(\overline{m}_t)$ (which would constitute differences at the level of 10 GeV) are unfounded. Furthermore, there is overall agreement in the demand that MMCs need to be improved to gain a higher level of precision concerning the quality of their PSs and hadronization models to reduce systematic uncertainties. For the second view, such improved precision is necessary to determine $\Delta_{m_t}^{\mathrm{MC}}(R_0, Q_0)$ from first principles analyses, but clearly all methods to determine the top mass would benefit from such improvements.

[12] An explicit computation gives $m_t^{\mathrm{pole}} - m_t^{\mathrm{MSR}}(R_0 = 1.3\ \mathrm{GeV}) = 360 \pm 250$ MeV for finite charm and bottom masses (47) (see **Figure 5**).

5. RECENT DEVELOPMENTS

5.1. Numerical Size of the Interpretation Problem

While initially only qualitative arguments for the interpretation problem for m_t^{MC} were available (12, 16, 18, 148, 149), some recent quantitative studies have shed light on the numerical aspect of the issue. In Reference 150, a combined analysis using the direct method and a pole mass measurement using the inclusive cross section indicated that $m_t^{\mathrm{pole}} - m_t^{\mathrm{MC}}$ is not larger than 2 GeV. In Reference 151, the numerical relations $m_t^{\mathrm{MC}} = m_t^{\mathrm{pole}} + (0.57 \pm 0.29)$ GeV and $m_t^{\mathrm{MC}} = m_t^{\mathrm{MSR}}$ (1 GeV) + (0.18 ± 0.23) GeV were obtained from fitting an NNLL+NLO calculation for the two-jettiness distribution in the resonance region for boosted top production in e^+e^- annihilation (76) to Pythia 8.2 (92) pseudodata samples. The result of this calibration study included a rigorous estimate of nonperturbative uncertainties of the analytic NNLL+NLO calculation, since hadronization corrections can be rigorously described by a factorized shape function (152). An analogous analysis for the LHC was performed in Reference 78 using soft-drop groomed (146) jet mass distributions at NLL+LO, obtaining compatible but less precise results.

The results of the analyses in References 150 and 151 are consistent with the view that the interpretation problem for m_t^{MC} is limited to the level of 0.5 to 1 GeV. Reference 151 also provided valuable quantitative results concerning the two views of Equations 13 and 14. In particular, the term $\Delta_{m_t}^{\mathrm{MC}}$ in Equation 13 has been shown to be about 0.5 GeV (i.e., of the same size as the uncertainties quoted for the LHC direct top mass measurements) for an e^+e^- process where Pythia (and all major MMCs) can be trusted to perform with a much higher precision. It is therefore conservative to conclude that the error in identifying m_t^{MC} with the pole mass is of at least the same size as the direct measurement uncertainties quoted by the experimental collaborations. Furthermore, the small difference between m_t^{MC} and m_t^{MSR} (1 GeV) supports the view that m_t^{MC} and the MSR mass at a low scale are closely related. This situation motivates the study of $\Delta_{m_t}^{\mathrm{MC}}(R_0, Q_0)$ in Equation 14 from first principles as well as work generalizing the e^+e^- result for boosted top quarks toward top production at the LHC. In Reference 24, such a first principles study was initiated for boosted top quark production in e^+e^- annihilation. I review the results of this study in the following section.

5.2. First Conceptual Insights

The relation between the MMC top mass parameter and the pole mass can be written as

$$m_t^{\mathrm{MC},Q_0} = m_t^{\mathrm{pole}} + \Delta_{\mathrm{MC}}^{\mathrm{pert}}(Q_0) + \Delta_{\mathrm{MC}}^{\mathrm{nonpert}}(Q_0) + \Delta^{\mathrm{MC}}. \qquad 15.$$

This equation presents a generalized unbiased version of Equations 13 and 14 that makes the potential shower cut dependence of the MMC top mass parameter explicit and visualizes the issues that need to be understood. As written, none of the three Δ terms on the right-hand side are accessible via the error estimates carried out by the experimental collaborations. The three Δ terms may even have different signs. Furthermore, all quantities except the pole mass m_t^{pole} are in principle MMC-dependent, which is indicated by the subscript and superscript letters MC. The term $\Delta_{\mathrm{MC}}^{\mathrm{pert}}(Q_0)$ represents perturbative corrections starting at $\mathcal{O}(\alpha_s)$ related to the (kind of) PS and the PS cutoff used by the MMC. The sum $m_t^{\mathrm{pole}} + \Delta_{\mathrm{MC}}^{\mathrm{pert}}(Q_0)$ can be written in any top mass scheme; thus, for the intended conceptual discussion, it does not matter which scheme is used. The pole mass can be used here because it is mostly used for fixed-order calculations. The term $\Delta_{\mathrm{MC}}^{\mathrm{nonpert}}(Q_0)$, which refers to possible effects coming from the MMC hadronization model that affect the meaning of m_t^{MC,Q_0}, should not be confused with the nonperturbative corrections that the hadronization model generates in the description of physical observables. It carries an argument Q_0 because it may depend on the PS setup if the PS does not carry a definite precision consistent

with QCD. The term Δ^{MC} encodes shifts due to MMC-related systematic uncertainties, which are physically unrelated to the dynamics of the top quark but may indirectly affect the theoretical meaning of the top mass parameter. Effects contributing to Δ^{MC} may include, for instance, effects from color reconnection or the b jet modeling and may be observable-dependent. If different measurements of m_t^{MC} were inconsistent, it would be evidence that $\Delta_{\mathrm{MC}}^{\mathrm{nonpert}}(Q_0)$ and Δ^{MC} are sizable for state-of-the-art MMCs. In a perfect MMC that made parton-level calculations consistent with QCD to subleading order and had hadronization models that were fully consistent with QCD for all processes, $\Delta_{\mathrm{MC}}^{\mathrm{nonpert}}(Q_0)$ as well as Δ^{MC} would be negligibly small, and m_t^{MC,Q_0} would be observable-independent. We could then simply calculate $\Delta_{\mathrm{MC}}^{\mathrm{pert}}(Q_0)$ from an analytic solution of the PS algorithm (with finite Q_0) for a simple mass-sensitive observable and a comparison with the corresponding partonic QCD calculation. In the analysis of Reference 151 (see Section 5.1), the sum of the three Δ terms was quantified as (0.57 ± 0.28) GeV for the Pythia 8.2 MMC and the e^+e^- two-jettiness distribution, but no information on the size and interplay of $\Delta_{\mathrm{MC}}^{\mathrm{pert}}(Q_0)$, $\Delta_{\mathrm{MC}}^{\mathrm{nonpert}}(Q_0)$, and Δ^{MC} was acquired. Such a differentiated knowledge is mandatory to allow for first principles conclusions regarding the field-theoretic interpretation of the Monte Carlo top mass m_t^{MC} because sizable contributions from $\Delta_{\mathrm{MC}}^{\mathrm{nonpert}}(Q_0)$ and Δ^{MC} can make the meaning of m_t^{MC,Q_0} observable-dependent and nonuniversal.

In Reference 24, a first principles study of Equation 15 was initiated through a dedicated analysis of the perturbative contribution $\Delta_{\mathrm{MC}}^{\mathrm{pert}}(Q_0)$. It was based on a combined analytical and numerical examination of the CB formalism for massive quarks (153) that is the theoretical basis of the angular-ordered PS used in the Herwig 7 MMC. The analysis was restricted in several ways:

1. The observable considered was the two-jettiness event shape distribution for boosted top pair production in e^+e^- annihilation in the resonance region, which is a global observable and equivalent to the distribution of the sum of the squared hemisphere masses with respect to the thrust axis. For this observable, the available NNLL+NLO QCD computation (76, 151) is based on a factorization of large-angle soft radiation (i.e., radiation that is soft in the $t\bar{t}$ center-of-mass frame) and ultracollinear radiation (i.e., radiation that is soft in the respective resonance frames of the boosted top quarks) (152). The results can therefore be immediately generalized to all e^+e^- massive quark event shape–type observables for which the ultracollinear dynamics is universal, but not to those employed for LHC top mass measurements.
2. The use of an e^+e^- event shape variable such as two-jettiness represents another physical restriction because the distribution is sensitive only to QCD radiation in the production stage of the top quarks, whereas the effect of final-state radiation (off the top decay products) is power-suppressed.
3. The NWA was employed, which does not account for finite-lifetime effects.
4. The angular-ordered CB shower formalism was considered, which differs from the transverse-momentum-ordered dipole shower formalism.

In this context, the following statements have been proven by first principles computations and by analytic as well as numerical studies:

> **Statement 1.** The consistent resummation of logarithms at NLL order in the singular resonance region, which carries the kinematic mass sensitivity, is mandatory and sufficient to control the top mass scheme with NLO [$\mathcal{O}(\alpha_s)$] precision.
>
> **Statement 2.** The CB formalism for massive quarks (153), and thus also the angular-ordered PS in Herwig 7, is NLL precise in the top mass–sensitive singular resonance region and is fully equivalent to the NLL′ QCD factorization predictions of References 76 and 151.

Statement 3. For vanishing infrared regularization (i.e., $Q_0 = 0$), the quark mass parameter appearing in the CB formalism at NLL order (defined in an expansion in powers of α_s and logarithms) agrees with the pole mass $m_t^{\rm pole}$ to NLO [i.e., $\mathcal{O}(\alpha_s)$]. This agreement does not, however, apply to angular-ordered PSs because their evolution requires a finite shower cut $Q_0 > \Lambda_{\rm QCD}$ to avoid infinite parton multiplicities and the strong coupling Landau pole.

Statement 4. In angular-ordered PSs, the shower cut Q_0 represents the minimal transverse momentum $p_\perp$ of radiated gluons or other partons that emerge from the showering and splittings. It also can be seen as a resolution scale or an infrared cutoff. An analysis of large-angle soft radiation as well as ultracollinear radiation with respect to linear effects in Q_0 was carried out for the PS and the QCD calculation. The analysis used a finite Q_0 for the PS and imposed the Q_0 cut in the QCD calculation in the pole scheme while also accounting for the mass counterterm (which is absent in the CB algorithm[13]). For the large-angle soft radiation, the linear Q_0 cutoff dependence is physical and represents a factorization scale at the interface to the nonperturbative effects [which is known as the linear power correction α_0 (154) or Ω_1 (155) in the tail of e^+e^- event shape distributions]. A change in Q_0 must therefore be compensated for by a corresponding modification of nonperturbative contributions and does not effectively lead to a change at the hadron level. For the ultracollinear radiation, terms that are linear in Q_0 are generated as well, but in the full QCD calculation their cumulative effect in a smeared distribution or a moment cancels such that there is no physical net effect. However, the finite Q_0 value entails that all virtual (self-energy and nonself-energy) ultracollinear radiation effects become unresolved and cancel[14] so that the pole of the top propagator is shifted away from $m_t^{\rm pole}$ (defined in the usual way without any infrared cut; recall the discussion in Section 2.2 after Equation 10) by a term that is linear in Q_0. This shifted mass of the top propagator pole, which has been called the CB mass, reads

$$m_t^{\rm CB}(Q_0) = m_t^{\rm pole} - \frac{2}{3}\,\alpha_s(Q_0)\,Q_0 + \ldots. \qquad 16.$$

The existence of a linear term in Q_0 on the right-hand side of this equation has precisely the same origin as the linear gluon mass term shown in Equation 5. Because the CB algorithm does not generate any self-energy corrections, the generator mass for finite Q_0 and at the parton level is equal to $m_t^{\rm CB}(Q_0)$ rather than $m_t^{\rm pole}$, which implies $\Delta^{\rm pert}_{\rm CB,Herwig}(Q_0) = -\frac{2}{3}\alpha_s(Q_0)Q_0$. For boosted top quarks, the linear effects in Q_0 on the large-angle soft and ultracollinear radiation have an opposite sign, but they also have a different dependence with respect to the center-of-mass energy Q. Thus, they can be analytically and numerically disentangled unambiguously at the parton level. These linear contributions correctly exponentiate so that the mass change is consistently implemented in the resummed tower of logarithms.

Statement 5. The CB mass $m_t^{\rm CB}(Q_0)$ is a short-distance mass, and therefore its relation to other short-distance masses is not affected by the pole mass renormalon ambiguity. For example, the numerical relation between the CB mass and the MSR mass reads $m_t^{\rm MSR}(Q_0) - m_t^{\rm CB}(Q_0) = 120 \pm 70$ MeV for the Herwig 7 shower cut $Q_0 = 1.25$ GeV, where 70 MeV is an estimate of the missing two-loop correction. This allows one to relate the CB mass to all other known short-distance masses with the same precision. Perturbation theory

[13] This issue is subtle and a potential source of misinterpretation.

[14] I refer to the cancellation of linear ultracollinear quantum corrections mentioned in Section 2.2 after Equation 7 and before Equation 9.

also works well at a scale of 1.25 GeV (which is close to the charm quark mass). Reducing this perturbative uncertainty would require determining the $\mathcal{O}(\alpha_s^2)$ term in Equation 16 in the context of an NNLL precise CB algorithm. The difference between the CB mass and the pole mass can be determined using the relation between the MSR mass and the pole mass shown in Footnote 12. This gives $m_t^{\text{pole}} - m_t^{\text{CB}}(Q_0) = 480 \pm 260$ MeV, which can be considered an all-order relation that cannot be made more precise.

What can we learn from the results of the analysis? First, I have some comments concerning its restrictions. The restriction to boosted top quarks goes hand-in-hand with the fact that both the CB formalism for massive quarks (153) (as well as dipole-type shower algorithms) and the QCD factorization approach of Reference 76 apply only in the quasi-collinear regime. For slow top quarks, a QCD factorization approach disentangling the individual top quarks from each other does not exist, and the use of branching algorithms is an extrapolation (even though no serious problems seem to appear in the top event description provided by MMCs). Therefore, conceptual and analytic first principles studies of the top quark generator mass for the bulk top quarks are, strictly speaking, impossible with the current set of theoretical tools, and one has to rely on extrapolation studies starting from the boosted regime. This limitation makes precision studies and top mass measurements with boosted top quarks, which become available with high statistics at the HL-LHC, interesting (for recent CMS and ATLAS measurements, see References 156–158). As mentioned above, the restriction to a global e^+e^- dijet event shape in the resonance region (where the top decay is treated fully inclusively) entails sensitivity to QCD radiation only in the production stage of the top quarks. Corresponding global event shape observables at the LHC are considerably more involved because of the effects of initial-state radiation underlying event contamination and long-distance color correlations. For boosted top quarks, however, the basic simplicity of QCD factorized predictions for e^+e^- collisions can also be largely maintained in hadron–hadron collisions if soft-drop groomed jet mass observables are considered (78, 159); thus, an LHC study analogous to Reference 24 is not unfeasible. Furthermore, e^+e^- dijet event shapes differ conceptually from the observables employed in the direct measurements, which use observables that are differential in the top decay. This restriction can be lifted by considering more differential observables, and technology to do so is available from the vast knowledge obtained through the theory of B meson decays (42, 43) and contemporary progress in factorized calculations (160). The soft-drop groomed top jet mass analysis in Reference 78 also goes in that direction but considers an observable that has not been analyzed to date by the experimental collaborations. The restriction to the NWA has been applied because state-of-the-art PSs do not provide a systematic treatment of the top quark width. The Herwig 7 generator uses the NWA, and Pythia is based on an NWA supplemented by throwing a random top mass value around the nominal top generator mass following a distribution of the Breit–Wigner type. In Reference 119, it was shown that using different approaches to treat the top decay and finite-lifetime effects can affect a top mass determination at the level of 0.5 or even 1 GeV, so this restriction is a very serious one. For the two-jettiness QCD calculation, the treatment of the leading finite-width effects is well understood (152). Finally, the restriction to the CB formalism was chosen as it is designed to work well for global observables and allows for a straightforward analytic solution and comparison with the predictions of QCD factorization. This restriction can in principle be lifted through a dedicated study of the dipole shower formalism, which is more elaborate analytically.[15]

[15] In Reference 161, a pure numerical analysis of the Q_0 dependence of the e^+e^- two-jettiness distribution was carried out using the dipole-type PS implementation of Reference 162. The numerical results were found to be consistent with the statements described in Statement 4 above.

It is clear that these restrictions need to be lifted to resolve the interpretation problem for contemporary direct top quark mass measurements, but they also reflect the limitations in principle of the state-of-the-art MMCs, which should be remedied. Furthermore, definite knowledge regarding the nonperturbative terms $\Delta_{\rm MC}^{\rm nonpert}(Q_0)$ and $\Delta^{\rm MC}$ needs to be gained. One way to do so is an analysis of the physical aspects of the hadronization models used in MMC from the perspective of observables for which definite statements on the first principles QCD structure of hadronization corrections are available. Each of the restrictions, as well as each of the nonperturbative terms, may have a numerical impact at the level of a few hundred MeV to 0.5 GeV. The results obtained in Reference 24 are therefore only a first step. The numerical analysis of Equation 16 demonstrates that the partonic contribution in Equation 15 is already of the size of the uncertainties quoted for current LHC direct mass measurements and that detailed analyses of all the terms on the right-hand side of Equation 15 are mandatory. To the extent that the infrared behavior of PS algorithms for ultracollinear radiation is universal and NLL precise, results of the kind shown in Equation 16, which applies to Herwig 7, should be observable-independent and applicable to other MMCs, although more studies are needed to substantiate this view.

The minimal aspect to be learned from the analysis of Reference 24 is that the identification of the direct mass measurements with the pole mass is field-theoretically incorrect. There is clear evidence that the additional error associated with making the identification is of at least the same size as the quoted experimental direct measurement uncertainties. Furthermore, because of the different structure of the evolution variables of different PS algorithms, it seems natural that the physical meaning of the top mass parameters in different PSs should not be assumed to be universal. Overall, the analysis affirms that more highly developed and more precise MMCs (with respect to NLL accurate PSs and finite-lifetime effects) are a necessary requirement to resolve the top mass interpretation problem.

6. SUMMARY AND RECOMMENDATIONS

In this review, I have presented an overview of the problems regarding how to interpret the direct top mass measurements, which quote the Monte Carlo top mass parameter $m_t^{\rm MC}$, from a physical and conceptual perspective. They touch perturbative (PSs and finite-width effects) as well as nonperturbative aspects and limitations of MMCs, and each may amount to effects at the level of several hundred MeV to half a GeV. Many of them go beyond the reach of the standard approaches used in high-energy collider physics today and require some novel avenues beyond the current paradigm of achieving higher theoretical precision by using MMCs matched to fixed-order perturbative computations. The top mass interpretation problem expresses the demand that, to measure theoretically defined QCD parameters at hadron colliders, MMCs themselves must provide first principles QCD predictions that are accurate to subleading order in QCD to control the renormalization scheme of their QCD parameters. This is not the case for state-of-the-art MMCs.

For the observables used in the direct measurement, for which the top mass sensitivity is tied to kinematic threshold structures, the PS algorithms should have NLL precision, and the hadronization models employed should implement nonperturbative effects consistent with QCD and the electroweak theory. For the top quark mass, the radiation that is soft in a top quark resonance frame plays the most important role. It is probably unrealistic to ask for this level of precision for all observables. However, for a number of key observables leading to high-precision top mass measurements with control over the mass scheme at NLO, such an achievement may be realistic in the near future. The relation of the MMC top mass parameter to any mass scheme and the question of universality and observable independence could then be obtained from computations rather than

from speculations. Developments in the direction of NLL precise PSs are already underway—for instance, concerning a more precise description of the parton splitting (163–165), the restriction of dipole-type showers for global observables (166, 167), finite-lifetime effects (168), and full color coherence (169, 170)—but there is still a long way to go.

How should one deal with the top mass interpretation problem today? It is well understood that the m_t^{MC} parameter obtained from direct top mass measurements is numerically close (i.e., within 0.5 or maybe 1 GeV) to mass schemes that are compatible with the top Breit–Wigner resonance. Such mass schemes include the pole mass m_t^{pole} and the MSR mass $m_t^{\mathrm{MSR}}(R)$ for scales R in the range of 1 to 2 GeV (i.e., close to the PS cutoff in MMCs and the top quark width Γ_t). Such mass schemes do not include the $\overline{\mathrm{MS}}$ mass $\overline{m}_t(\overline{m}_t)$ in QCD. In the analysis of Reference 24, the parton-level relations between the top mass parameter $m_t^{\mathrm{CB}}(Q_0)$ in the angular-ordered PS of Herwig 7 and the pole and MSR masses were computed analytically for an e^+e^- observable, where the PS was shown to have NLL precision. The relation $m_t^{\mathrm{CB}}(Q_0) - m_t^{\mathrm{pole}} = -\frac{2}{3}\,\alpha_s(Q_0)\,Q_0$ was derived, and $m_t^{\mathrm{CB}}(Q_0)$ was shown to be a short-distance mass. Numerically, the results give $m_t^{\mathrm{pole}} - m_t^{\mathrm{CB}}(Q_0) = 480 \pm 260$ MeV and $m_t^{\mathrm{MSR}}(Q_0) - m_t^{\mathrm{CB}}(Q_0) = 120 \pm 70$ MeV, where $Q_0 = 1.25$ GeV is the Herwig 7 shower cutoff. In the work described in Reference 151, the observable employed in Reference 24 was used to determine the corresponding relations numerically at the hadron level by a calibration fit using an NNLL+NLO QCD calculation yielding $m_t^{\mathrm{MC}} - m_t^{\mathrm{pole}} = 570 \pm 290$ MeV and $m_t^{\mathrm{MC}} - m_t^{\mathrm{MSR}}$ (1 GeV) $= 0.180 \pm 230$ MeV for Pythia 8.2. These results show that the nonperturbative aspects of the interpretation problem also are relevant for state-of-the-art direct top mass measurements, which have reached a precision of 0.5 GeV. Clearly, a deeper understanding is crucial to obtain a reliable and systematic high-precision top mass measurement at the HL-LHC. Much work is needed to analyze the extent to which the dynamical effects of the hadronization models affect the meaning of m_t^{MC} and to carry out similar analyses for observables closer to those used in the LHC measurements.

To date, there is no general consensus on how to quantify the interpretation problem of the direct top mass measurements for making mass-dependent theoretical predictions. It is left to the individual to decide how to deal with this issue. I hope that this review provides readers a deeper insight to inform this choice. Most often, the identification $m_t^{\mathrm{MC}} = m_t^{\mathrm{pole}}$ is made, sometimes supplemented by adding another uncertainty on the order of the quoted experimental uncertainty. If this approach is adopted, I recommend—as a practical attitude (neither very conservative nor very optimistic) for the time being—adding an uncertainty of 0.5 GeV to account for the interpretation problem plus 250 MeV to account for the pole mass renormalon ambiguity. As an additional option, which accounts for the existing evidence that the MMC top masses are short-distance masses and reflects a somewhat less conservative attitude, I recommend using the identification $m_t^{\mathrm{MC}} = m_t^{\mathrm{MSR}}$ (1.3 GeV), adding an uncertainty of 0.5 GeV to quantify the interpretation problem. In this approach, the pole mass renormalon ambiguity is brought back in the conversion to m_t^{pole} for predictions made in the pole mass scheme (the outcome just differs by a 350-MeV shift in the central value with respect to the first approach). However, the pole mass renormalon ambiguity is avoided completely when considering only predictions made in short-distance mass schemes. In this context, one should employ the method explained in Section 2.2 to convert between pole and short-distance masses.

DISCLOSURE STATEMENT

The author is not aware of any affiliations, memberships, funding, or financial holdings that might be perceived as affecting the objectivity of this review.

ACKNOWLEDGMENTS

I thank my collaborators Mathias Butenschoen, Bahman Dehnadi, Sean Fleming, Ambar Jain, Christopher Lepenik, Sonny Mantry, Vicent Mateu, Aditya Pathak, Simon Plätzer, Moritz Preisser, Daniel Samitz, Ignazio Scimemi, Maxi Stahlhofen, and Iain Stewart for their valuable contributions to work important to this review. I thank Katerina Lipka, Marcel Vos, and the editor for comments and suggestions regarding the manuscript. I acknowledge partial support from the FWF Austrian Science Fund under the Doctoral Program ("Particles and Interactions") No. W1252-N27, as well as Projects P28535-N27 and P32383-N27, and from the European Union under the COST action ("Unraveling new physics at the LHC through the precision frontier") No. CA16201. I thank Simon Plätzer for providing **Figures 6** and **7** and Christopher Lepenik for providing all other figures.

LITERATURE CITED

1. Tanabashi M, et al. (Part. Data Group) *Phys. Rev. D* 98:030001 (2018)
2. Azzi P, et al., eds. *Standard Model Physics at the HL-LHC and HE-LHC*. Geneva: CERN. **https://e-publishing.cern.ch/index.php/CYRM/article/view/950** (2019)
3. Higgs PW. *Phys. Rev. Lett.* 13:508 (1964)
4. Englert F, Brout R. *Phys. Rev. Lett.* 13:321 (1964)
5. Guralnik GS, Hagen CR, Kibble TWB. *Phys. Rev. Lett.* 13:585 (1964)
6. Cabibbo N, Maiani L, Parisi G, Petronzio R. *Nucl. Phys. B* 158:295 (1979)
7. Alekhin S, Djouadi A, Moch S. *Phys. Lett. B* 716:214 (2012)
8. Buttazzo D, et al. *J. High Energy Phys.* 1312:89 (2013)
9. Andreassen A, Frost W, Schwartz MD. *Phys. Rev. Lett.* 113:241801 (2014)
10. Branchina V, Messina E. *Phys. Rev. Lett.* 111:241801 (2013)
11. Isidori G, Ridolfi G, Strumia A. *Nucl. Phys. B* 609:387 (2001)
12. Hoang AH, Stewart IW. *Nucl. Phys. Proc. Suppl.* 185:220 (2008)
13. Moch S, Langenfeld U, Uwer P. *Proc. Sci.* RADCOR2009:030 (2010)
14. Deliot F, Glenzinski DA. *Rev. Mod. Phys.* 84:211 (2012)
15. Juste A, et al. *Eur. Phys. J. C* 74:3119 (2014)
16. Moch S, et al. arXiv:1405.4781 [hep-ph] (2014)
17. Corcella G. *EPJ Web Conf.* 80:00019 (2014)
18. Hoang AH. arXiv:1412.3649 [hep-ph] (2014)
19. Weinzierl S. arXiv:1505.00630 [hep-ph] (2015)
20. Boos E, et al. *Phys. Usp.* 58:1133 (2015) [*Usp. Fiz. Nauk* 185:1241 (2015)]
21. del Duca V, Laenen E. *Int. J. Mod. Phys. A* 30:1530063 (2015)
22. Corcella G. *Proc. Sci.* TOP2015:037 (2016)
23. Azzi P, et al. arXiv:1703.01626 [hep-ph] (2017)
24. Hoang AH, Plätzer S, Samitz D. *J. High Energy Phys.* 1810:200 (2018)
25. Fadin VS, Khoze VA. *Sov. J. Nucl. Phys.* 48:309 (1988) [*Yad. Fiz.* 48:487 (1988)]
26. Strassler MJ, Peskin ME. *Phys. Rev. D* 43:1500 (1991)
27. Jezabek M, Kuhn JH, Teubner T. *Z. Phys. C* 56:653 (1992)
28. Hoang AH, et al. *Eur. Phys. J. Direct* 2:3 (2000)
29. Hoang AH, Stahlhofen M. *J. High Energy Phys.* 1405:121 (2014)
30. Beneke M, et al. *Phys. Rev. Lett.* 115:192001 (2015)
31. Seidel K, Simon F, Tesar M, Poss S. *Eur. Phys. J. C* 73:2530 (2013)
32. Horiguchi T, et al. arXiv:1310.0563 [hep-ex] (2013)
33. Vos M, et al. arXiv:1604.08122 [hep-ex] (2016)
34. Abramowicz H, et al. (CLICdp Collab.) *J. High Energy Phys.* 11:3 (2019)
35. Boronat M, et al. *Phys. Lett. B* 804:135353 (2020)
36. Tarrach R. *Nucl. Phys. B* 183:384 (1981)

37. Gray N, Broadhurst DJ, Grafe W, Schilcher K. *Z. Phys. C* 48:673 (1990)
38. Chetyrkin KG, Steinhauser M. *Phys. Rev. Lett.* 83:4001 (1999)
39. Chetyrkin KG, Steinhauser M. *Nucl. Phys. B* 573:617 (2000)
40. Melnikov K, Ritbergen TV. *Phys. Lett. B* 482:99 (2000)
41. Marquard P, Mihaila L, Piclum JH, Steinhauser M. *Nucl. Phys. B* 773:1 (2007)
42. Neubert M. *Phys. Rep.* 245:259 (1994)
43. Manohar AV, Wise MB. *Heavy Quark Physics*. Cambridge, UK: Cambridge Univ. Press (2000)
44. Ball P, Beneke M, Braun VM. *Nucl. Phys. B* 452:563 (1995)
45. Baak M, et al. (Gfitter Group) *Eur. Phys. J. C* 74:3046 (2014)
46. Buras AJ. *Phys. Lett. B* 317:449 (1993)
47. Hoang AH, Lepenik C, Preisser M. *J. High Energy Phys.* 1709:99 (2017)
48. Aaboud M, et al. (ATLAS Collab.) *Eur. Phys. J. C* 79:290 (2019)
49. Foldy LL, Wouthuysen SA. *Phys. Rev.* 78:29 (1950)
50. Hoang AH, Jain A, Scimemi I, Stewart IW. *Phys. Rev. Lett.* 101:151602 (2008)
51. Hoang AH, et al. *J. High Energy Phys.* 1804:3 (2018)
52. Voloshin MB. *Phys. Rev. D* 46:3062 (1992)
53. Bigi I, Shifman M, Uraltsev N. *Annu. Rev. Nucl. Part. Sci.* 47:591 (1997)
54. Czarnecki A, Melnikov K, Uraltsev N. *Phys. Rev. Lett.* 80:3189 (1998)
55. Hoang AH, Ligeti Z, Manohar AV. *Phys. Rev. Lett.* 82:277 (1999)
56. Hoang AH, Ligeti Z, Manohar AV. *Phys. Rev. D* 59:074017 (1999)
57. Hoang AH. *Phys. Rev. D* 61:034005 (2000)
58. Beneke M. *Phys. Lett. B* 434:115 (1998)
59. Pineda A. *J. High Energy Phys.* 0106:022 (2001)
60. Jain A, Scimemi I, Stewart IW. *Phys. Rev. D* 77:094008 (2008)
61. Marquard P, Smirnov AV, Smirnov VA, Steinhauser M. *Phys. Rev. Lett.* 114:142002 (2015)
62. Lehmann H, Symanzik K, Zimmermann W. *Nuovo Cim.* 1:205 (1955)
63. Lehmann H, Symanzik K, Zimmermann W. *Nuovo Cim.* 6:319 (1957)
64. Kronfeld AS. *Phys. Rev. D* 58:051501 (1998)
65. Bigi II, Shifman MA, Uraltsev NG, Vainshtein AI. *Phys. Rev. D* 50:2234 (1994)
66. Beneke M, Braun VM. *Nucl. Phys. B* 426:301 (1994)
67. Beneke M. *Phys. Rep.* 317:1 (1999)
68. Gross DJ, Neveu A. *Phys. Rev. D* 10:3235 (1974)
69. Lautrup B. *Phys. Lett. B* 69:109 (1977)
70. 't Hooft G. *Subnucl. Ser.* 15:943 (1979)
71. David F. *Nucl. Phys. B* 234:237 (1984)
72. Mueller AH. *Nucl. Phys. B* 250:327 (1985)
73. Smith MC, Willenbrock SS. *Phys. Rev. Lett.* 79:3825 (1997)
74. Peset C, Pineda A, Segovia J. *J. High Energy Phys.* 1809:167 (2018)
75. Beneke M, Marquard P, Nason P, Steinhauser M. *Phys. Lett. B* 775:63 (2017)
76. Fleming S, Hoang AH, Mantry S, Stewart IW. *Phys. Rev. D* 77:114003 (2008)
77. Ferrario Ravasio S, Nason P, Oleari C. *J. High Energy Phys.* 1901:203 (2019)
78. Hoang AH, Mantry S, Pathak A, Stewart IW. *Phys. Rev. D* 100:074021 (2019)
79. Incandela JR, Quadt A, Wagner W, Wicke D. *Prog. Part. Nucl. Phys.* 63:239 (2009)
80. Schilling FP. *Int. J. Mod. Phys. A* 27:1230016 (2012)
81. CMS Collab. *Projected improvement of the accuracy of top-quark mass measurements at the upgraded LHC*. CMS Phys. Anal. Summ. CMS-PAS-FTR-13-017, CERN, Geneva (2013)
82. Corcella G. *Front. Phys.* 7:54 (2019)
83. Czakon M, Fiedler P, Heymes D, Mitov A. *J. High Energy Phys.* 1605:34 (2016)
84. Czakon M, et al. *J. High Energy Phys.* 1805:149 (2018)
85. Czakon M, et al. *J. High Energy Phys.* 1710:186 (2017)
86. Gao J, Li CS, Zhu HX. *Phys. Rev. Lett.* 110:042001 (2013)
87. Gao J, Papanastasiou AS. *Phys. Rev. D* 96:051501 (2017)

88. Heinrich G, et al. *J. High Energy Phys.* 1406:158 (2014)
89. Denner A, Pellen M. *J. High Energy Phys.* 1802:13 (2018)
90. Langenfeld U, Moch S, Uwer P. *Phys. Rev. D* 80:054009 (2009)
91. Bellm J, et al. *Eur. Phys. J. C* 76:196 (2016)
92. Sjöstrand T, et al. *Comput. Phys. Commun.* 191:159 (2015)
93. Gleisberg T, et al. *J. High Energy Phys.* 0902:007 (2009)
94. Dasgupta M, et al. *J. High Energy Phys.* 1809:33 (2018)
95. Cormier K, et al. *Eur. Phys. J. C* 79:915 (2019)
96. Marchesini G, Webber BR. *Nucl. Phys. B* 238:1 (1984)
97. Nagy Z, Soper DE. *J. High Energy Phys.* 0510:024 (2005)
98. Plätzer S, Gieseke S. *J. High Energy Phys.* 1101:24 (2011)
99. Webber BR. *Nucl. Phys. B* 238:492 (1984)
100. Andersson B, Gustafson G, Ingelman G, Sjöstrand T. *Phys. Rep.* 97:31 (1983)
101. Frixione S, Webber BR. arXiv:hep-ph/0207182 (2002)
102. Alwall J, et al. *J. High Energy Phys.* 1407:79 (2014)
103. Alioli S, Nason P, Oleari C, Re E. *J. High Energy Phys.* 1006:43 (2010)
104. Plätzer S, Gieseke S. *Eur. Phys. J. C* 72:2187 (2012)
105. Hoeche S, Krauss F, Schonherr M, Siegert F. *J. High Energy Phys.* 1209:49 (2012)
106. Bellm J, et al. *Eur. Phys. J. C* 76:665 (2016)
107. Bendavid J, et al. arXiv:1803.07977 [hep-ph] (2018)
108. Ferrario Ravasio S, Jeo T, Nason P, Oleari C. *Eur. Phys. J. C* 78:458 (2018)
109. Bellm J, et al. arXiv:1705.06919 [hep-ph] (2017)
110. Gieseke S, Rohr C, Siodmok A. *Eur. Phys. J. C* 72:2225 (2012)
111. Argyropoulos S, Sjöstrand T. *J. High Energy Phys.* 1411:43 (2014)
112. Christiansen JR, Skands PZ. *J. High Energy Phys.* 1508:3 (2015)
113. Gieseke S, Kirchgaeßer P, Plätzer S. *Eur. Phys. J. C* 78:99 (2018)
114. Gieseke S, Kirchgaeßer P, Plätzer S, Siodmok A. *J. High Energy Phys.* 1811:149 (2018)
115. Sjöstrand T, Skands PZ. *Eur. Phys. J. C* 39:129 (2005)
116. Bahr M, Gieseke S, Seymour MH. *J. High Energy Phys.* 0807:076 (2008)
117. Corcella G, Franceschini R, Kim D. *Nucl. Phys. B* 929:485 (2018)
118. Jeo T, et al. *Eur. Phys. J. C* 76:691 (2016)
119. Heinrich G, et al. *J. High Energy Phys.* 1807:129 (2018)
120. Sirunyan AM, et al. (CMS Collab.) *Eur. Phys. J. C* 79:313 (2019)
121. Sirunyan AM, et al. (CMS Collab.) *Eur. Phys. J. C* 77:354 (2017)
122. Tevatron Electroweak Work. Group (CDF–D0 Collab.) arXiv:1407.2682 [hep-ex] (2014)
123. Abazov VM, et al. (D0 Collab.) *Phys. Rev. D* 91:112003 (2015)
124. Siikonen H. arXiv:2002.06073 [hep-ex] (2020)
125. Czakon M, Fiedler P, Mitov A. *Phys. Rev. Lett.* 110:252004 (2013)
126. Alioli S, et al. *Eur. Phys. J. C* 73:2438 (2013)
127. Frixione S, Mitov A. *J. High Energy Phys.* 1409:12 (2014)
128. Aad G, et al. (ATLAS Collab.) *Eur. Phys. J. C* 74:3109 (2014). Addendum. *Eur. Phys. J. C* 76:642 (2016)
129. Khachatryan V, et al. (CMS Collab.) *J. High Energy Phys.* 1608:29 (2016)
130. Sirunyan AM, et al. (CMS Collab.) *Eur. Phys. J. C* 79:368 (2019)
131. Alekhin S, Blümlein J, Moch S, Placakyte R. *Phys. Rev. D* 96:014011 (2017)
132. Dulat S, et al. *Phys. Rev. D* 93:033006 (2016)
133. Harland-Lang LA, Martin AD, Motylinski P, Thorne RS. *Eur. Phys. J. C* 75:204 (2015)
134. Ball RD, et al. (NNPDF Collab.) *Eur. Phys. J. C* 77:663 (2017)
135. Aad G, et al. (ATLAS Collab.) *J. High Energy Phys.* 1911:150 (2019)
136. Aaboud M, et al. (ATLAS Collab.) *Eur. Phys. J. C* 77:804 (2017)
137. Sirunyan AM, et al. (CMS Collab.) arXiv:1904.05237 [hep-ex] (2019)
138. Lester CG, Summers DJ. *Phys. Lett. B* 463:99 (1999)
139. Chatrchyan S, et al. (CMS Collab.) *Eur. Phys. J. C* 73:2494 (2013)

140. Agashe K, Franceschini R, Kim D, Schulze M. *Eur. Phys. J. C* 76:636 (2016)
141. Khachatryan V, et al. (CMS Collab.) *J. High Energy Phys.* 1612:123 (2016)
142. Khachatryan V, et al. (CMS Collab.) *Phys. Rev. D* 93:092006 (2016)
143. Butterworth JM, Davison AR, Rubin M, Salam GP. *Phys. Rev. Lett.* 100:242001 (2008)
144. Ellis SD, Vermilion CK, Walsh JR. *Phys. Rev. D* 81:094023 (2010)
145. Krohn D, Thaler J, Wang LT. *J. High Energy Phys.* 1002:84 (2010)
146. Larkoski AJ, Marzani S, Soyez G, Thaler J. *J. High Energy Phys.* 1405:146 (2014)
147. Kawabata S, Yokoya H. *Eur. Phys. J. C* 77:323 (2017)
148. Nason P. *Proc. Sci.* TOP2015:056 (2016)
149. Nason P. arXiv:1712.02796 [hep-ph] (2017)
150. Kieseler J, Lipka K, Moch SO. *Phys. Rev. Lett.* 116:162001 (2016)
151. Butenschoen M, et al. *Phys. Rev. Lett.* 117:232001 (2016)
152. Fleming S, Hoang AH, Mantry S, Stewart IW. *Phys. Rev. D* 77:074010 (2008)
153. Gieseke S, Stephens P, Webber B. *J. High Energy Phys.* 0312:045 (2003)
154. Davison RA, Webber BR. *Eur. Phys. J. C* 59:13 (2009)
155. Abbate R, et al. *Phys. Rev. D* 83:074021 (2011)
156. Sirunyan AM, et al. (CMS Collab.) *Eur. Phys. J. C* 77:467 (2017)
157. Aaboud M, et al. (ATLAS Collab.) *Phys. Rev. D* 98:012003 (2018)
158. Sirunyan AM, et al. (CMS Collab.) arXiv:1911.03800 [hep-ex] (2019)
159. Hoang AH, Mantry S, Pathak A, Stewart IW. *J. High Energy Phys.* 12:2 (2019)
160. Becher T, Broggio A, Ferroglia A. Introduction. In *Introduction to Soft-Collinear Effective Theory*, pp. 1–4. Cham, Switz.: Springer (2015)
161. Baumeister R, Weinzierl S. arXiv:2004.01657 [hep-ph] (2020)
162. Dinsdale M, Ternick M, Weinzierl S. *Phys. Rev. D* 76:094003 (2007)
163. Li HT, Skands P. *Phys. Lett. B* 771:59 (2017)
164. Höche S, Prestel S. *Phys. Rev. D* 96:074017 (2017)
165. Dulat F, Höche S, Prestel S. *Phys. Rev. D* 98:074013 (2018)
166. Dasgupta M, et al. arXiv:2002.11114 [hep-ph] (2020)
167. Forshaw JR, Holguin J, Plätzer S. arXiv:2003.06400 [hep-ph] (2020)
168. Brooks H, Skands P. *Phys. Rev. D* 100:076006 (2019)
169. Ángeles Martínez R, et al. *J. High Energy Phys.* 1805:44 (2018)
170. Forshaw JR, Holguin J, Plätzer S. *J. High Energy Phys.* 1908:145 (2019)

Annual Review of Nuclear and Particle Science

Volume 70, 2020

Contents

Errata

An online log of corrections to *Annual Review of Nuclear and Particle Science* articles may be found at http://www.annualreviews.org/errata/nucl